Technische Universität München
TUM School of Medicine and Health

Pten deletion blocks PDK1-loss induced growth arrest of pancreatic cancer cells

Lukas Josef Neudegger

Vollständiger Abdruck der von der TUM School of Medicine and Health der Technischen Universität München zur Erlangung eines

Doktors der Medizin (Dr. med.)

genehmigten Dissertation.

Vorsitz: Prof. Dr. Gabriele Multhoff

Prüfende der Dissertation:

1. Prof. Dr. Dieter Saur
2. Prof. Dr. Radu Roland Rad

Die Dissertation wurde am 04.09.2023 bei der Technischen Universität München eingereicht und durch die TUM School of Medicine and Health am 09.04.2024 angenommen.

Table of contents

List of tables

2. List of figures

3. List of abbreviations

°C	degrees celsius
µl	microliter
4-OHT	4-hydroxytamoxifen
ANOVA	analysis of variance
APS	ammonium persulfate
bp	base pair
BSA	bovine serum albumin
CENP-C	centromere-specific binding protein C
CRISPR	clustered regularly interspaced short palindromic repeats
d	day
ddH_2O	double-destilled water
DMEM	Dulbecco´s modified Eagle medium
DNA	deoxyribonucleic acid
dNTP	deoxynucleoside triphosphate
DRS	dual-recombinase system
DTT	dithiothreitol
ERK	extracellular signal-related kinase
EtOH	ethanol
FBS	fetal bovine serum
Foxo	forkhead box O protein
FSF	frt-stop-frt
GAP	GTPase-activating protein
GDP	guanosine diphosphate
GEF	guanine nucleotide exchange factor
GEMM	genetically engineered mouse model
GTP	guanosine triphosphate
h	hour
HDR	homology directed repair
HEK	human embryonic kidney
IP	immune-precipitation

kDa	kilo Dalton
KO	knock-out
LB	Luria Broth Bertani
MapK	mitogen-activated protein kinase
min	minute
ml	milliliter
mTOR	mammalian target of rapamycin
mV	millivolt
NHEJ	non-homologous end joining
nMol	nanomole
PAM	protospacer adjacent motif
PanIN	pancreatic intraepithelial neoplasia
PBS	phosphate buffered saline
PCR	polymerase chain reaction
PDAC	pancreatic ductal adenocarcinoma
PDK1	3-phosphoinositide-dependent protein kinase 1
PH	pleckstrin homology
Pi3k	phosphoinositide 3-kinase
PIP2	phosphatidylinositol 4,5-bisphosphate
PIP3	phosphatidylinositol 3,4,5-trisphosphate
PKB	protein kinase B
PKC	protein kinase C
Pten	phosphatase and tensin homolog
rpm	revolutions per minute
RTK	receptor tyrosine kinase
SDS PAGE	sodium dodecyl sulphate-polyacrylamide gel electrophoresis
Sgk	serum- and glucocorticoid-regulated kinases
sgRNA	single guide RNA
TEA	tris-acetate EDTA
TEMED	tetramethylethylendiamin
Tsc2	Tuberous Sclerosis Complex 2

4. Abstract

Of all pancreatic malignancies, pancreatic ductal adenocarcinoma (PDAC) is the most common at more than 90%, making it the most prevalent of all pancreatic neoplastic diseases. Today, it represents the fourth leading cause of cancer-related death, worldwide. Genetically engineered mouse models (GEMMs) have enabled scientists to investigate molecular, histological and clinical hallmarks of PDAC. Recently developed transgenic mouse models with a dual recombinase system (DRS) allow controlled genetic modeling and manipulation of sequential multistep tumorgenesis. Our group previously showed that PDK1 is essential for KRAS-driven pancreatic cancer growth and maintenance making it a putative therapeutic target in future cancer treatment. However, few cell clones resisted PDK1 deletion. A genetic CRISPR/CAS9 knockout (KO) screen revealed numerous potential genes whose deletion compensated growth arrest in PDK1-deficient PDAC cells; including the tumor suppressor *Pten.* In this dissertation a murine model with a DRS allowing us to subsequently delete PDK1 was used to investigate the in vitro effect of PTEN-KO in PDK1-deficient cells. Clonogenic assays as well as flow cytometry based cell cycle assays showed a significant rescue effect after KO of PTEN, thereby validating PTEN-loss as a mechanism to survive PDK1 deletion induced growth arrest in PDAC cells. The quantitative protein analysis of PTEN-KO cells indicates that compensatory changes in PI3K/AKT signaling, such a p-AKT and mTOR upregulation, likely contribute to their resistance. To validate the molecular mechanism, further experiments will be necessary.

5. Introduction

5.1 Pancreatic ductal adenocarcinoma (PDAC)

Patients diagnosed with PDAC are facing the poor 5-year survival rate of less than 8% and a mean survival time of six to eight months (Gillen, Schuster et al. 2010, Orth, Metzger et al. 2019). Today, PDAC represents the fourth-leading death related cancer diagnosis worldwide (Orth, Metzger et al. 2019). Because the available diagnostic tests are lacking in specificity, they may miss patients with early-stage disease (Rawla, Sunkara et al. 2019). In fact, only 20% of the affected patients present with operable stages of carcinoma whereas the remaining 80% are diagnosed with advanced and inoperable stages or often distant metastases (Orth, Metzger et al. 2019). Smoking, obesity, diabetes or alcohol consumption represent well-known risk factors for this entity of cancer (Rawla, Sunkara et al. 2019).

Usually as the first-line treatment, systemic chemotherapy using nucleoside analogues as a monotherapy, in combination with other chemo therapeutics or other therapeutic modalities like radiotherapy are applied. In the last decade an increased incidence and mortality rate of pancreatic cancer was recorded. Despite persistent research in this field, PDAC still has an incident/mortality ratio of 94% (Bray, Ferlay et al. 2018, Rawla, Sunkara et al. 2019) which emphasizes the urge to find specific therapies for affected patients.

5.2 Oncogenic KRAS signaling

KRAS is a small GTPase, which normally changes between a GTP-bound active and a GDP-bound inactive mode. This switch between the two states of activity is controlled by guanine nucleotide exchange factors (GEFs), which lead to an active state by stimulating the exchange of GDP for GTP and by GTPase activating proteins (GAPs), which lead to an inactive state by stimulating GTP hydrolysis (Scheffzek K. and Kabsch W. 1997, Vigil, Cherfils et al. 2010). KRAS activation in healthy cells is a result of extracellular stimulation of receptor tyrosine kinases (RTKs) and other membrane receptors by growth factors (Waters and Der 2018). It plays an important role for cell cycle progression, proliferation and survival as it stimulates multiple effector signaling pathways like the RAF/MEK/extracellular signal-related kinase (ERK), also known as mitogen-activated protein kinase (MAPK) pathway, and the phosphoinositide 3-kinase (PI3K)/phosphoinositide-dependent kinase 1 (PDK1)/AKT axis

(**Figure 1**). These represent the main signaling pathways in PDAC (Campbell, Groehler et al. 2007, Ferro and Falasca 2014, Waters and Der 2018). Activating mutations of *Kras* can be found frequently in human lung, colon or pancreatic cancer (Cox and Der 2010, Cox, Fesik et al. 2014). A study showed that activating mutations of the proto-oncogene *Kras* were found nearly ubiquitously in PDAC (Waddell, Pajic et al. 2015). Most mutations in PDAC alter a glycine at amino acid 12 to an aspartate or valine amino acid (*Kras*^{G12A} or *Kras*^{G12D} respectively) leading to steric clashes, which then block the interaction of KRAS with GAPs. This terminates GTP hydrolysis, resulting in a state of constitutively active KRAS (Scheffzek K. and Kabsch W. 1997, Ferro and Falasca 2014). There are numerous KRAS downstream effector pathways described. In the following, the PI3K/PDK1/AKT pathway is described in detail.

5.3 The PI3K/PDK1/AKT axis

Phosphoinositide 3-kinase signaling plays an important role in a variety of cellular processes like migration, cell growth, proliferation or survival (Canley 2002). Grouped into three classes, eight mammalian PI3K enzymes are described. Class I PI3K enzymes (PI3Kα, PI3Kβ, PI3Kγ and PI3Kδ) are heterodimers consisting of a regulatory and a catalytic subunit. For class I, four catalytic subunits of 110 kDa can be differentiated respectively: p110α p110β, p110γ and p110δ (Fruman and Rommel 2014). The regulating subunit mediates the activation ofthe catalytic p110 subunit when interacting with phosphotyrosine residues of activated growth factor receptors. When active, PI3K catalyzes the phosphorylation of the membrane lipid phosphatidylinositol (4, 5)-biphosphate (PIP2) to phosphatidylinositol (3, 4, 5)-triphosphate (PIP3). This reaction is reversed by the phosphatase and tensin homologue (Pten), which thereby inactivates PI3K signaling. Proteins with a pleckstrin-homology (PH) domain interact with PIP_3 by directly binding to it. Important downstream effectors of PI3K are the phosphoinositide-dependent kinase 1 (PDK1) and AKT both representing serine-threonine kinases. With their PH domains, PDK1 and AKT bind PIP_3 and get recruited to the cellular membrane in proximity, which enables the phosphorylation of AKT at threonine 308 (T308) by PDK1 (Alessi, Deak et al. 1997, Canley 2002, Kikani, Dong et al. 2005). This allows

AKT to be phosphorylated at its serine residue 473 (S473) and thus being fully activated by mammalian target of rapamycin complex 2 (mTorC2) (Emmanouilidi, Fyffe et al. 2019, Shi, Wang et al. 2019). Activated AKT subsequently phosphorylates many other target proteins thereby regulating multiple cellular functions like promoting cell metabolism, cell cycle progression, survival and protein synthesis: AKT down-regulates forkhead (FOXO) family of transcription factors, TSC2 as well as glycogen synthase kinase 3 (GSK3). Additionally, the pro-apoptotic protein Bad can directly be phosphorylated by AKT, which leads to its inactivation (Engelman, Luo et al. 2006). It was shown that induction of pancreas specific oncogenic PI3K signaling in mouse models lead to sequential step tumorgenesis. Histopathological anaylsis showed ADM developing to PanIN-3 representing carcinoma in situ (Eser, Reiff et al. 2013). This data emphasizes the relevance of PI3K signaling in PDAC.

5.4 PDK1 in PDAC

PDK1, a 63 kDa protein (Stephens, Anderson et al. 1998), plays a critical role in the PI3K/AKT pathway as described above. Besides contributing to full activation of AKT downstream of PI3K, PDK1 functions as a master kinase phosphorylating and activating many other members of the AGC kinases, such as S6K, SGK or some PKC isoforms (Raimondi and Falasca 2011). Having in mind that in 97% of human PDAC oncogenic KRAS is found (Cox, Fesik et al. 2014), PDK1 represents an attractive target protein in pancreatic cancer (Emmanouilidi, Fyffe et al. 2019) as it is a key downstream effector of KRAS (Raimondi and Falasca 2011, Ferro and Falasca 2014). The Saur lab showed in a previous study that *Pdk1* inactivation in both allels entirely impaired PanIN and PDAC formation in Murine $Kras^{G12D}$ models, whereas PanIN and PDAC formation was not blocked only deleting one *Pdk1* allel. To demonstrate whether PDK1/PI3K signaling might serve as a target in PDAC therapy, an oral selective PI3K inhibitor (GDC 0941) was applied which inhibited growth of murine $Kras^{G12D}$ driven PDAC and human derived PDAC cells in vitro. Furthermore GDC 0941 treatment stabilized cancer growth in vivo, whereas control mice showed rapid tumor progression (Eser, Reiff et al. 2013).

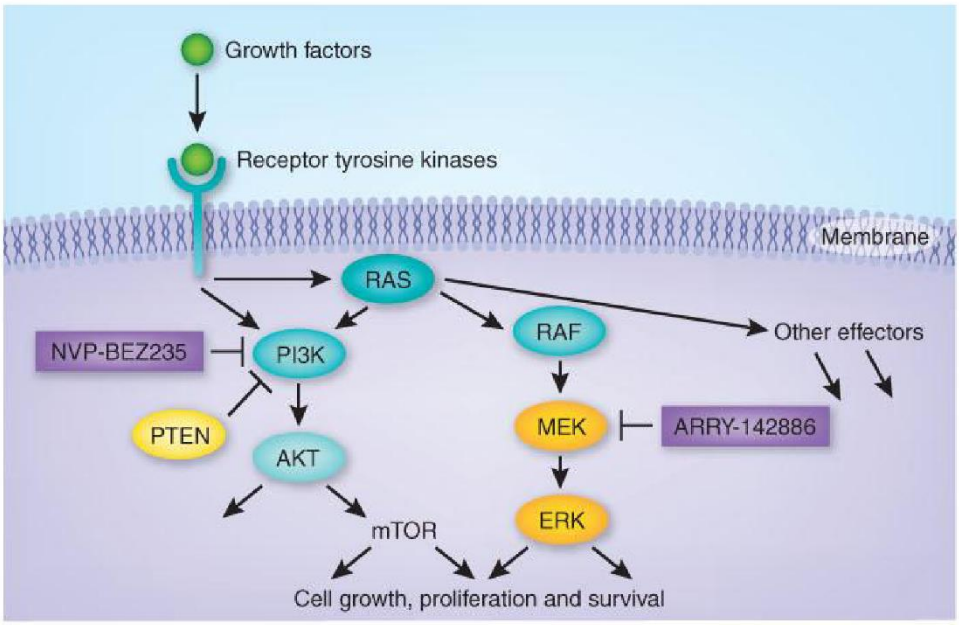

Figure 1. The PI3K and MAPK signaling pathways function as downstream effector pathways of RAS. Stimulated by growth factors, receptor tyrosine kinases activate RAS, leading to an activation of the PI3K/AKT signaling pathway as well as the RAF/MEK/ERK signaling pathway, promoting cell growth, proliferation and survival (Downward 2008).

Reprinted by permission from Springer Nature: Nature Medicine (Downward 2008)

5.5 PTEN

The tumor suppressor phosphatase and tensin homologue deleted on chromosome 10 (PTEN) is a dual lipid and protein phosphatase, which is commonly altered in human cancer cells. The protein is known for its function in antagonizing the PI3K pathway by dephosphorylating its primary substrate PIP_3 to PIP_2. (**Figure 2**). Consequently, the second messenger PIP_3 cannot fulfill its functions such as recruiting AKT to the cellular membrane where it would be activated. Thus, PTEN is inhibiting cell growth, survival and proliferation by antagonizing the PI3K/AKT axis (Hopkins, Hodakoski et al. 2014, Milella, Falcone et al. 2015). Also nuclear functions of this protein are described. In the nucleus it promotes genomic stability (Hopkins, Hodakoski et al. 2014) via interaction with

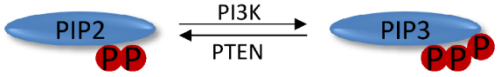

Figure 2. PTEN reverses the catalytic reaction of PI3K

the centromere-specific binding protein C (CENP-C) (Shen, Balajee et al. 2007). Additionally, PTEN plays a role in cell cycle progression, by decreasing nuclear Cyclin D1 level (Milella, Falcone et al. 2015). It has been demonstrated that down regulation of PTEN is common in human PDAC. Ying, Elpek et al. reported in their study from 2011 that 70% of their PDAC-samples showed no or low PTEN-expression in comparison to the surrounding stroma. Furthermore, this tumor suppressor seems to promote *Kras*^{G12D}-driven pancreatic cancer. A study revealed an accelerated and also intensified phenotype of acinar-to-ductal metaplasia (ADM) as well as malignant progression in *Kras*$^{G12D/+}$ *Pten*-KO mice (Hill, Calvopina et al. 2010).

5.6 Genome editing with CRISPR/CAS9

To study the function of a gene, a common approach in research is to shut down the gene or to over express it. The term “clustered regularly interspaced short palindromic repeats (CRISPR)/CRISPR-associated (CAS) protein 9” describes a system which allows researchers to knock out (KO) genes encoding for specific proteins (Zhang, Wen et al. 2014). CRISPR/CAS9 was discovered in bacteria and archaea functioning as an acquired immune system against viruses and plasmids (Jinek, Chylinski et al. 2012). In this endogenous system, the Cas nuclease processes foreign DNA into small fragments which then can be integrated as spacers into the CRISPR locus. In case of a virus or phage infection, these spacers can be used as templates for producing CRISPR targeting RNA (crRNA) guiding the CAS endonuclease together with the trans-activating RNA (tracRNA) to the invading DNA, which then is cleaved and thus rendered harmless (Zhang, Wen et al. 2014, Zhan, Rindtorff et al. 2019). The CRISPR/CAS system is classified into three types (I, II, III). System II, which only needs a single CAS protein for DNA cleavage (CAS9) has been shown to be an effective and simple tool in genome editing (Zhang, Wen et al. 2014). Also the development of a single guide RNA (sgRNA) instead of the endogenous combination of crRNA and tracrRNA further simplified the system. The 20 bp sgRNA sequence together with the precedent three nucleotide protospacer adjacent motif (PAM) sequence ensures binding specificity at the targeted sequence. Then, two nuclease domains implement a double strand break at this DNA locus. This damage causes the host cell to response with one of two repair mechanisms,

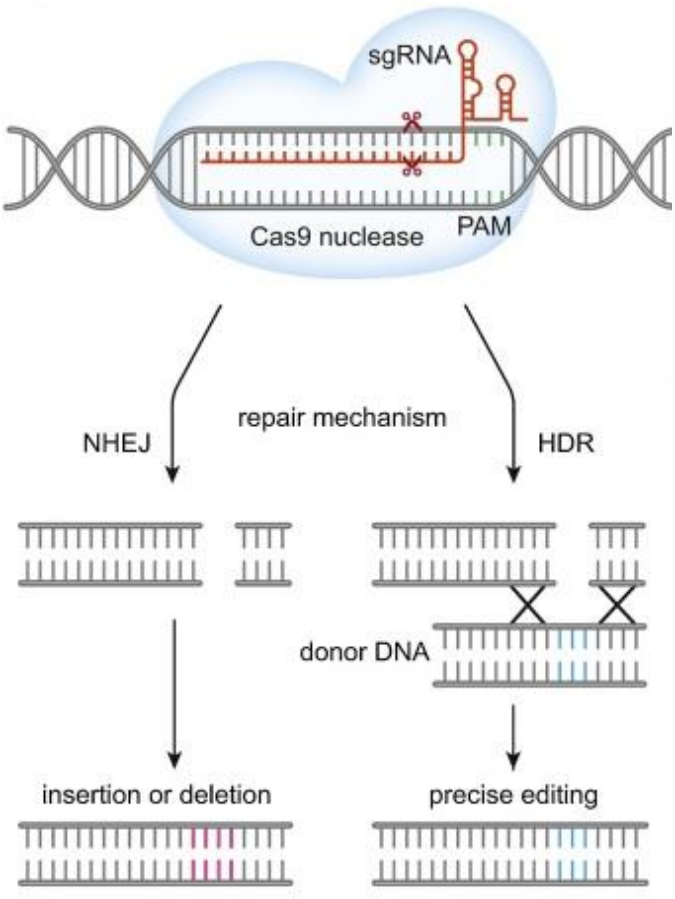

Figure 3. The CRISPR/CAS9 system enables targeted genome editing
CAS9 endonuclease is guided to its target DNA sequence by the sgRNA where it cleaves the DNA resulting in a double strand break. The host cell reacts to this damage with repair mechanisms: Non homologous end joining (NHEJ), causing random insertions/deletions or homology directed repair (HDR), which enables precise editing using a donor DNA template. (Zhan, Rindtorff et al. 2019) Adapted from Zhan et al. 2019, Seminars in Cancer Biology, Elsevier

non homologues end joining (NHEJ) or homology directed repair (HDR, **Figure 3**). The defective NHEJ mechanism often causes insertions or deletions (indels) in the genome. These indels can lead to frameshift mutations, stop codon insertions or nonsense mutations, resulting in a loss of function of the protein encoded by the affected gene. HDR reconstitutes cleaved DNA via assisted recombination of DNA donor templates. This mechanism allows researchers to integrate a precise mutation by introducing donor DNA templates to the targeted cell (Zhan, Rindtorff et al. 2019). The CRISPR/CAS9 technique enables pooled genetic screens in a genome-wide manner (Doench 2018).

5.7 A Murine model for controlled *Pdk1*-deletion

To investigate effects of a *Pdk1* deletion in pancreatic cancer cells, an adequate Murine model is necessary. Classical Cre-*loxP*-based mouse models have been developed, but they only allow a single step recombination which can be used to activate oncogenic KRAS expression to generate tumor mice. The Saur lab developed a new generation of genetically engineered mouse models (GEMMs) enabling the opportunity to genetically validate

possible targets or resistance mechanisms of PDAC. The dual recombinase system (DRS) of this GEMM is based on the FLP- and CRE-recombinase. Mice with the genotype *Pdx1-Flp*;FSF-*Kras*$^{G12D/+}$;FSF-R26$^{CAG\text{-}CreERT2}$;*Pdk1*$^{lox/lox}$ were created. The FLP-recombinase which is controlled by the *Pdx1* promoter in this model recombines and deletes the *frt*-flanked stop cassettes before the oncogenic *Kras*^{G12D} and the 4-hydroxytamoxifen (4-OHT)-inducible CreER^{T2} (**Figure 4**). Consequently, the mice are expressing oncogenic KRAS^{G12D} leading to PDAC formation. Additional CreER^{T2} expression allows recombining the *loxP*-flanked *Pdk1*-locus by treating the mice with 4-OHT. To accelerate PDAC formation mice with additionally deactivated tumor suppressor *p53* were generated using a *frt*-flanked *Trp53* allele (Schonhuber, Seidler et al. 2014). The cell lines used in this study for in vitro experiments were generated in Dieter Saurs lab from pancreatic tumors of DRS-mice.

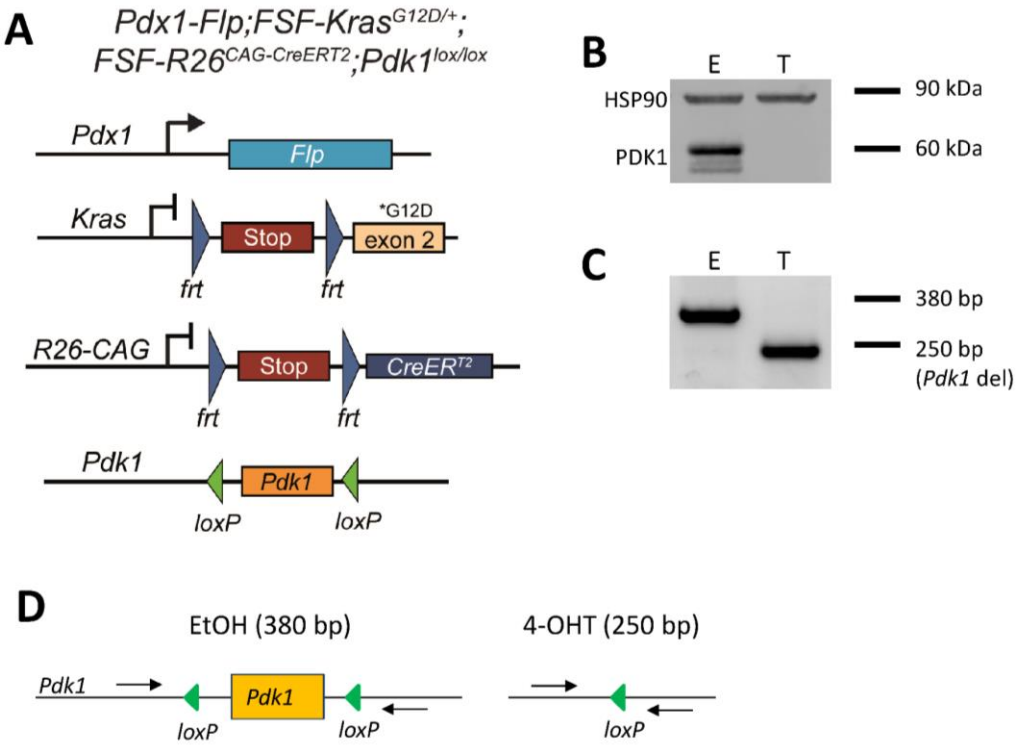

Figure 4. A dual recombinase system (DRS) mouse model enables expression of oncogenic KRAS and controlled deletion of PDK1

A Under control of the *Pdx1* promoter, Flp is expressed and removes the stop-cassetes, so oncogenic Kras^{G12D} and CreER^{T2} get expressed. If 4-OHT is added, CRE is activated and the l*oxP* flanked *Pdk1* allele gets recombined (Schönhuber et al., 2014). **B** The protein immunoblot shows the deletion of Pdk1 in 4-OHT-treated cells (T). In the EtOH-control (E) the Pdk1-specific band is still visible. A 8-day treatment with 4-OHT or EtOH was used. Hsp90 served as a loading control. **C**, **D** Recombination of the *Pdk1* locus was controlled via PCR.

5.8 Aim of this work

This work targets the question whether depletion of *Pten* can compensate a *Pdk1* deletion in Murine PDAC cells. A study of the Saur group showed that PDK1 is indispensable for PDAC formation and thus a promising putative target for pancreatic cancer therapy therapy (Schonhuber, Seidler et al. 2014). However, PDK1-independent clones could be isolated from Murine PDAC cells (unpublished data by C. Veltkamp, Ag Saur). This leads to the question of why some cancer cells are not dependent of PDK1 and which mechanisms this resistance is underlying. Deletion of both *Pdk1* alleles resulted in normal life expectancy and showed no signs of PDAC or pancreatic intraepithelial neoplasias (PanIN), which are precursor lesions of PDAC. However, inactivation of only one *Pdk1* allele did not prevent PanIN and PDAC formation (Eser, Reiff et al. 2013). The Saur lab with K. Sleiman (PHD candidate) used a genome wide CRISPR/CAS9 knockout enrichment screen to target this question. Multiple hit genes were found whose deletion seemed to cause an independence of *Pdk1*; including the tumor suppressor PTEN (**Figure 2**). This dissertation targets the question whether depletion of PTEN can compensate a PDK1 deletion in Murine PDAC cells.

6. Material

Table 1. Technical equipment

Device	Source
Analytical balance BP610	Sartorius AG, Göttingen
Bacteria incubator	Heraeus GmbH, Hanau
Bag sealer Folio FS 3602	Severin Elektrogeräte GmbH, Sundern
Centrifuge 5427 R	Eppendorf AG, Hamburg
CO_2 incubator HERAcell®	Fisher Scientific GmbH, Schwerte
Electrophoresis power supply 1	Analytik Jena GmbH, Jena
Electrophoresis power supply 2	Bio-Rad Laboratories GmbH, Munich
Gel Doc™ XR+ System	Bio-Rad Laboratories GmbH, Munich
Gel electrophorsis system	Analytik Jena GmbH, Jena
Glass ware, Schott Duran®	Schott AG, Mainz
HERAsafe® bilogical safety cabinet	Thermo Fisher Scientific Inc., Waltham, USA
Horizontal gel electrophoresis system	Analytik Jena GmbH, Jena
Laminar flow Envair eco	Envair Deutschland GmbH, Emmendingen
Magnetic stirrer, Ikamag ® RCT	IKA® Werke GmbH & Co. KG, Staufen
Microcentrifuge 5415 D	Eppendorf AG, Hamburg
Microscope DMIL LED	Leica Microsystems GmbH, Wetzlar
Microwave	Imtron GmbH, Ingolstadt
Multifuge X3 FR	Fisher Scientific GmbH, Schwerte
Multipette stream	Eppendorf AG, Hamburg
Odyssey® infrared imaging system	Li-Cor Biosciences, Lincoln NE, USA
Orbital shaker	Carl Roth GmbH & Co. KG, Karlsruhe
Pipet controller Stripettor™	Corning Inc., Glendale, USA
Pipettes	Eppendorf AG, Hamburg
Spectrophotometer NanoDrop 1000	Pqlab Biotechnologie GmbH, Erlangen
Thermocycler “Biometra Tone“	Analytik Jena GmbH, Jena
Thermomixer compact	Eppendorf AG, Hamburg
Vortex Genie 2	Scientific Industries Inc., New York
Water bath 1003	GFL Gesellschaft für Labortechnik mbH, Burgwedel
Western blot system (Mini-Protean® Tetra System)	Bio-Rad Laboratories GmbH, Feldkirchen

Table 2. Disposables

Disposable	Source
Cell culture plastics	Becton Dickinson GmbH, Franclin Lakes, NJ, USA; Greiner Bio-One GmbH, Frickenhausen; TPP Techno Plastic Products AG, Trasadingen, Switzerland

Cell scrapers	Sarstedt® AG & Co. KG, Nürmbrecht
Combitips Advanced™	Eppendorf AG, Hamburg
Conical tubes, 15 mL, 50 mL	Falcon™ Fisher Scientific GmbH, Schwerte
Cryo tubes	Sarstedt® AG & Co. KG, Nürmbrecht
Filtropur S 0.45	Sarstedt® AG & Co. KG, Nürmbrecht
Nitrocellulose blotting membrane (0.2 µm) Amersham™ Protran®	Cytiva GmbH, Dassel
Pasteur pipettes	Hirschmann Laborgeräte GmbH & Co. KG, Eberstadt
PCR reaction tubes	Eppendorf AG, Hamburg
Petri dishes	Sarstedt® AG & Co. KG, Nürmbrecht
Pipette tips	Sarstedt® AG & Co. KG, Nürmbrecht
Reaction tubes, 0.25 ml, 0.5 mL, 1.5 mL and 2 mL	
Reaction tubes, 0.5 mL, 1.5 mL, 2 mL	Eppendorf AG, Hamburg
Safe-lock reaction tubes BioPur®	Eppendorf AG, Hamburg

Table 3. Reagents and enzymes

1 kb DNA extension ladder	Invitrogen GmbH, Karlsruhe
1,4-Dithiothreitol (DTT)	Carl Roth GmbH & Co. KG, Karlsruhe
2-Mercaptoethanol 98%	Sigma-Aldrich Chemie GmbH, Darmstadt
2-Propanol (isopropanol)	Carl Roth GmbH & Co. KG, Karlsruhe
4-hydroxytamoxifen	Sigma-Aldrich Chemie GmbH, Darmstadt
Agarose	Sigma-Aldrich Chemie GmbH, Darmstadt
Ammonium persulfate	SERVA Electrophoresis GmbH, Heidelberg
Ammonium persulfate	Sigma-Aldrich Chemie GmbH, Darmstadt
Ampicillin	Carl Roth GmbH & Co. KG, Karlsruhe
Blotting grade blocker non-fat dry milk	Bio-Rad laboratories GmbH, Munich
Bovine serum albumin	Sigma-Aldrich Chemie GmbH, Darmstadt
Bradford reagent	Serva Electrophoresis GmbH, Heidelberg
Bromphenol blue	Sigma-Aldrich Chemie GmbH, Darmstadt
BsmBI	New England Biolabs, Ipswich
Crystal violet	Sirchie, Youngsville, NC
Dimethylsulfoxide (DMSO)	Carl Roth GmbH & Co. KG, Karlsruhe
Dulbecco´s modified eagle medium (DMEM)	Sigma-Aldrich Chemie GmbH, Darmstadt
Dulbecco´s phosphate buffered saline (PBS)	Sigma-Aldrich Chemie GmbH, Darmstadt
Ethanol (100%)	Merck KGaA, Darmstadt
Ethidium bromide	Sigma-Aldrich Chemie GmbH, Darmstadt
Ethylenediaminetetraacetic acid (EDTA)	Invitrogen GmbH, Karsruhe
Fetal calf serum (FCS)	Sigma-Aldrich Chemie GmbH, Darmstadt
Glycerol	Sigma-Aldrich Chemie GmbH, Darmstadt
Glycin Pufferan®	Carl Roth GmbH & Co. KG, Karlsruhe
HEPES Pufferan®	Carl Roth GmbH & Co. KG, Karlsruhe
LB agar (Luria/Miller)	Carl Roth GmbH & Co. KG, Karlsruhe

LB broth (Luria/Miller)	Carl Roth GmbH & Co. KG, Karlsruhe
Methanol	Merck KGaA, Darmstadt
NaCl	Merck KGaA, Darmstadt
Nonidet P40	Roche Deutschland Holding GmbH, Grenzach-Wyhlen
Opti-MEM® reduced serum medium	Thermo Fisher Scientific, Dreieich
Penicillin/Streptomycin solution	Sigma-Aldrich Chemie GmbH, Darmstadt
Phosphatase inhibitor mix I	Serva Electrophoresis GmbH, Heidelberg
Proteinase K	PanReac AppliChem GmbH, Darmstadt
Puromycin dihydrochloride	Sigma-Aldrich Chemie GmbH, Darmstadt
REDTaq® ReadyMix™ PCR reaction mix	Sigma-Aldrich Chemie GmbH, Darmstadt
RnaseA	Sigma-Aldrich Chemie GmbH, Darmstadt
SDS pellets	Serva Electrophoresis GmbH, Heidelberg
T4 DNA Ligase	New England Biolabs, Ipswich
T4 DNA Ligase buffer	New England Biolabs, Ipswich
TAE buffer	Apotheke Klinikum Rechts der Isar, Munich
TEMED	Carl Roth GmbH & Co. KG, Karlsruhe
TransIT®-L T1	Mirus Bio LLC, Madison, USA
Tris Pufferan®	Carl Roth GmbH & Co. KG, Karlsruhe
Trypsin (TrypZean®)	Sigma-Aldrich Chemie GmbH, Darmstadt
Tween® 20	Carl Roth GmbH & Co. KG, Karlsruhe

Table 4. Antibodies

Antibody	**Source**
β-ACTIN	Cell Signaling Technology Cat# 4970, RRID:AB_2223172
AKT	Cell Signaling Technology Cat# 9272, RRID:AB_329827
Anti-mouse	Thermo Fisher Scientific Cat# SA5-35521, RRID:AB_2556774
Anti-rabbit	Thermo Fisher Scientific Cat# SA5-35571, RRID:AB_2556775
Cyclin D1	Cell Signaling Technology Cat# 55506, RRID:AB_2827374
FOXO1	Cell Signaling Technology Cat# 2880, RRID:AB_2106495
HSP90	Santa Cruz Biotechnology Cat# sc-13119, RRID:AB_675659
mTOR	Cell Signaling Technology Cat# 2983, RRID:AB_2105622
PDK1	Cell Signaling Technology Cat# 3062, RRID:AB_2236832
Phospho-AKT (S473)	Cell Signaling Technology Cat# 9271, RRID:AB_329825
Phospho-AKT (T308)	Cell Signaling Technology Cat# 2965, RRID:AB_2255933

Phospho-FOXO1 (S319)	Cell Signaling Technology Cat# 2487, RRID:AB_561444
Phospho-FOXO1 (T24)	Cell Signaling Technology Cat# 9464, RRID:AB_329842
Phospho-mTOR (S2481)	Cell Signaling Technology Cat# 2974, RRID:AB_2262884
Phospho-RICTOR (T1135)	Cell Signaling Technology Cat# 3806, RRID:AB_10557237
Phospho-S6 (S235-236)	Cell Signaling Technology Cat# 4858, RRID:AB_916156
Phospho-S6 (S240244)	Cell Signaling Technology Cat# 5364, RRID:AB_10694233
Phospho-SGK1 (S422)	Abcam Cat# ab55281, RRID:AB_882529
PTEN	Cell Signaling Technology Cat# 9188, RRID:AB_2253290
RICTOR	Cell Signaling Technology Cat# 2140, RRID:AB_2179961
S6	Cell Signaling Technology Cat# 2217, RRID:AB_331355
SGK1	Cell Signaling Technology Cat# 3272, RRID:AB_2239204

Table 5. Buffers

10x Gitschier´s buffer	670 mM Tris, pH 8.8 166 mM (NH4)2SO4 67 mM MgCl2
IP buffer	50 mM HEPES 150 mM NaCl 1 mM EDTA 0.5% Nonidet P40 10% Glycerol Phosphatase inhibitor (supplemented prior to use) Protease inhibitor (supplemented prior to use)
Running buffer	25 mM Tris 192 mM Glycine 0.1% SDS
Separating gel buffer	1.5 M Tris, adjusted to pH 8.8 with HCl
Soriano lysis buffer	0.5% Triton® X-100 1% 2-Mercaptoethanol 1x Gitschier's buffer 400 µg/mL Proteinase K (add prior to use)
Stacking gel buffer	0.5 M Tris, adjusted to pH 6.8 with HCl

Transfer buffer, pH 8.3	25 mM Tris 192 mM Glycine 20% Methanol
5x Protein loading buffer (Laemmli), pH 6.8	10% SDS 50% Glycerol 228 mM Tris hydrochloride 0.75 mM Bromphenol blue 5% 2-Mercaptoethanol
5x Protein loading buffer (Laemmli), ph 6.8	10% SDS 50% Glycerol 228 mM Tris hydrochloride 0.75 nM Bromphenol blue 5% 2-Mercaptoethanol

Table 6. Kits

Kit	Source
GenEluteTM Mammalian Genomic DNA Miniprep Kit	Sigma-Aldrich Chemie GmbH, Steinheim
Monarch® PCR % DNA cleanup Kit	New England Biolabs Ipswich, MA, USA
Plasmid Midi Kit	Quiagen, Hilden
QIAprep Spin Miniprep Kit	Quiagen, Hilden

Table 7. Bacterial strains

Bacterial strain	**Source**
Endura^{TM} chemically competent cells	Sigma-Aldrich Chemie GmbH, Darmstadt

Table 8. Plasmids

Lenti CRISPRv2 puro	Addgene, Cambridge, MA, USA
PsPAX	Addgene, Cambridge, MA, USA
PMD2.G	Addgene, Cambridge, MA, USA

Table 9. SgRNAs

sgRNA	**Sequence**	**Source**
PTEN_1	CCTCCAATTCAGGACCCACG	BRIE Library, Eurofins Genomics
PTEN_4	GGTTTGATAAGTTCTAGCTG	
Lac-z	TGCGAATACGCCCACGCGAT	
Non targeting	GGAGTGTTATACGCACCGTT	

Table 10. Primers

PCR	Primer	sequence	Source
Pten_1	Pten_1 fw Pten_1 rev	AAGGATTCAGATTGAAGAAGTCCT AATCAGTTTGGTAGATGGCAGAGA	Eurofins Genomics
Pten_4	Pten_4 fw Pten_4 rev	GCACAATGCTTGTTTCCATGTCT AGGGAGAAAACCTGTTTCCCAA	Eurofins Genomics
Pdk1-del	Pdk1-i4-UP2 Pdk1-del-UP Pdk1-LP	CCCTCTAGCAAATGTTCTGTCTGGAATGTCT CTATGCTGTGTTACTTCTTGGAGCACAG TGTGGACAAACAGCAATGAACATACACGC	Eurofins Genomics

Table 11. Cell culture medium

Medium	**Components**
Cancer cell medium	DMEM 10% FCS 1% Penicillin/Streptomycin
Freezing medium	70% DMEM 20% FCS 10% DMSO

Table 12. Software

Software	**Source**
Serial cloner	http://serialbasics.free.fr/, Freeware
Graphpad Prism 5	GraphPad Software, San Diego, CA, USA
TIDE	Bas van Steensel lab, Amsterdam, Netherlands
Excel	Microsoft Corporation, Redmont, WA, USA

7. Methods

7.1 Experiments with murine cells

7.1.1 Genotype

The cell lines CV7250 and V5213 (**Figure 5**) were established as primary pancreatic cancer cells from tumor mice with the genotype *Pdx1-Flp*;FSF-*Kras*$^{G12D/+}$;FSF-R26$^{CAG-CreERT2}$;*Pdk1*$^{lox/lox}$;p53-frt$^{+/+}$. These mouse line as well as the cell lines were established in the laboratory of Prof. Dr. Dieter Saur. It is assumed that the cell lines are polyclonal.

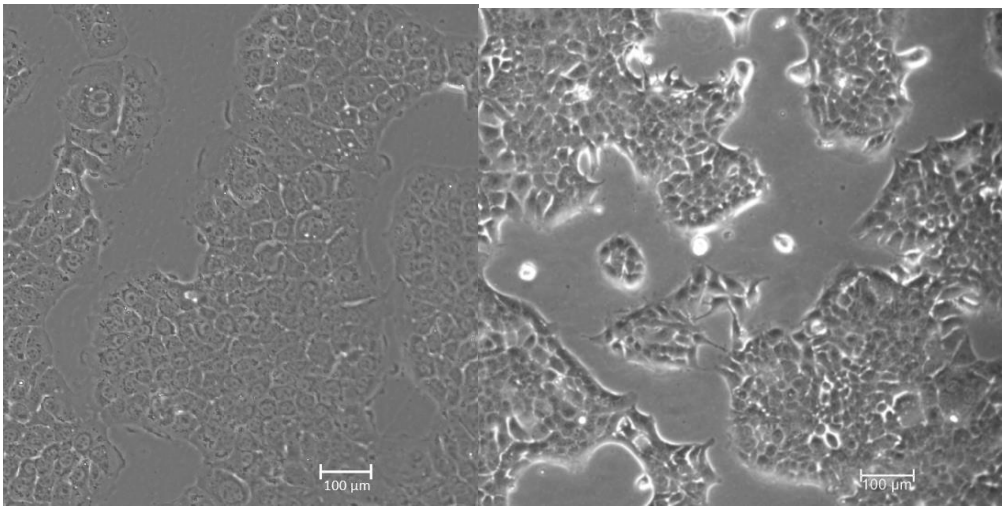

Figure 5. Primary pancreatic tumor cell lines CV7250 (left, taken by C. Veltkamp) and V5213 (right). The cell lines were established in the Saur lab.

Cells were cultured in cancer cell medium (DMEM containing 10% fetal bovine serum (FBS) and 1% penicillin-streptomycin) at 37 °C. For passaging, medium was aspirated and cells were washed with Dulbecco´s phosphate buffered saline (PBS). After aspirating PBS, trypsin was added to detach the cells from the plastic surface. Fresh medium was added to inactivate the trypsin and the cell suspension was moved to new flasks.

7.1.2 4-hydroxytamoxifen (4-OHT) and Ethanol (EtOH) treatment

To activate CreER^{T2} and to subsequently delete *Pdk1* cells were treated with 600 nMol 4-OHT respectively EtOH (control) for 8 days.

7.1.3 CellTiter Glo® assay

The CellTiter Glo® assay can be used to measure cell viability by indirectly measuring the ATP level of cells via luminescence.[1] 500 cells per well were seeded into 96-well plates as quadruplicates after previous treatment with 4-OHT to delete *Pdk1* or EtOH as a control. 25 µl of CellTiter Glow® reagent were added, and the plates were covered with aluminum foil to protect the reagent from light. Then, the plates were put onto an orbital shaker for 10 minutes at 100 rpm before measuring the luminescence at with the spectrophotometer. This assay was performed on five consecutive days.

7.1.4 Clonogenic assay

For the clonogenic assays, 2000 cells per well were seeded on a 6-well plate in triplicates. After 10-15 days of incubation, medium was aspirated and plates were washed one time with PBS. PBS was also discarded and 750 µl of a 0.2% crystal violet solution (**Table 13**) were added and incubated for one hour at room temperature. Afterwards the staining solution was thrown and plates were washed three times by submerging under tap water. Then the plates were left to dry overnight upside down on paper tissues. Subsequently, images of the plates were taken and the dye on the plates was solubilized with 1% SDS solution. Absorbance of the solubilized crystal violet was measured at 570 nm with the spectrophotometer to quantify colony formation.

Reagent	**Volume/mass**
Crystal violet	0.2 g
EtOH	2 ml
ddH_2O	98 ml

Table 13. Crystal violet solution for clonogenic assay staining.

[1] https://www.promega.de/

7.1.5 Cell cycle analysis

Cell cycle analysis based on DNA amount was carried out using flow cytometry. For the experiments, a paper (Hassan, Schneeweis et al. 2018) was used as a guidance. The cells were seeded in 10 cm-diameter cell culture plates. When around 70% confluent, cells were trypsinized and washed in PBS. The PBS-cell suspension was centrifuged (1000 rpm, 5 min) before discarding the supernatant and resuspending the cells in 70% EtOH for fixation. Also, the supernatant cell culture medium was aspirated, centrifuged (1000 rpm, 5 min) and washed with PBS. This step was included to also consider apoptotic cells in the analysis. Before the measurement, 25 µl/ml of propiumiodide as well as RNAse (final concentration 0.5 µg/ml) were added to the fixed cells and incubated for 30 min.

7.2 Genome editing with CAS9

7.2.1 Cloning of sgRNAs

To create PTEN-KO cells using CRISPR/CAS9 genome editing, two sgRNAs of the BRIE library (**Table 9**) were cloned seperately into a lentiCRISPRv2-puro plasmide backbone. For oligo annealing, 1 µl of the forward as well as of the reverse oligo (100µM) were mixed with 1 µl of T4 DNA Ligase Buffer (NEB) and 7 µl H_2O in an Eppendorf tube. The mixture was incubated at 95 °C in a heat block. Then, the tubes were left at room temperature for 30 min before diluting with 490 µl of H_2O. After the oligo annealing, the sgRNAs were cloned into the lentiCRISPRv2_puro vector. The corresponding reaction mix and thermocycler programm is listed in **Table 14**. After performing the thermocycler program, the assembled mix was used for transformation.

lentiCRISPRv2-puro (90µg/µl)	1 µl
Annealed and diluted oligo	1 µl
T4 DNA Ligase Buffer (10x)	2 µl
T4 DNA Ligase	1 µl
BsmBI restriction enzyme (10 000 units/mL)	1 µl
H_2O	14 µl

37°C	5 min	10x
16°C	10 min	
55°C	5 min	
80°C	5 min	
10°C	Pause	

Table 14. Mixture for the cloning procedure (left) and the corresponding thermocycler conditions (right).

7.2.2 Transformation of bacteria

To amplify plasmids containing the desired sgRNA chemically competent bacteria (Endura^{TM}) were transformed using KCM transformation. This techniqie uses a KCl, CaCl2 and MgCl2 solution to introduce foreign DNA into a bacterial cell. Therefore, 10 µl of the assembled mix from the cloning procedure was added to 20 µl KCM buffer and 70 µl H_2O. This transformation mix was added to 100 µl Endura^{TM}. The bacteria was incubated for 10 min on ice and for 10 min at room temperature afterwards. Then, 1 mL liquid Luria Broth Bertani (LB) medium was added to the bacteria before incubating for 1 h at 28 °C in the thermomixer at 1000 rpm to develop ampicillin resistance. The transformed bacteria was streaked out on LB agar plates containing ampicillin (100 µg/ml) and incubated overnight at 28 °C to select transformed clones. Then, single bacterial clones were picked and incubated in liquid LB medium. After the bacteria had replicated for 24 hrs, plasmids were prepped using SIGMA plasmid mini prepping kits. To insure that the selected clones were transformed with the desired plasmid correctly a diagnostic digest was performed. Therefore, DNA of the bacterial clone was incubated with BsmBI restriction enzyme at 55 °C for 2 hrs. Then the samples were analysed via agarose gel electropheresis. To confirm the sgRNA sequence plasmid samples were sent for sequencing and data was analyzed with Serial Cloner. After confirmation that the picked bacterial clone was transformed correctly,

bacteria was incubated in liquid LB medium again for 24 hrs. Then, plasmids were prepped using SIGMA plasmid midi prepping kits.

7.2.3 Lentivirus transfection

To edit the genome of the target cells using CAS9, the desired plasmid was packed into a lentivirus. The sgRNA plasmid and two lentiviral plasmids for packaging and envelope (PMD2.G, PsPAX) were incubated together with HEK293FT-cells. The HEK293FT-cells were seeded in 10 cm-dishes ($2x10^6$/dish). After 24 hrs a transfection mix was prepared: For each dish 1500 µl Opti-MEM® cell medium was mixed with 6.5 µg psPAX, 4.1 µg pMD2.G and 8.2 µg of the plasmid containing Pten_1 or Pten_4. Then, 55 µl of TransIT-LT1 were added as an enhancer. This mixture incubated at room temperature for 15-30 min before adding it drop wise to the 10 cm-dish. After rocking the dish for equal distribution, the HEK293FT cells were incubated at 37 °C. 24 hrs after, the old cell medium was exchanged with fresh medium. Another 24 hrs later, the viral supernatant was collected and filtered with a 0.45 µm filter before freezing at -80 °C.

7.2.4 Lentiviral transduction

Target cells for lentiviral transduction were seeded in 6-well plates (150 000cells per well). After 24 hrs, medium was aspirated and 200 µl of the filtered virus supernatant were added together with polybrene (final concentration 8 µg/ml). Then, the plates were placed into a centrifuge at 1000 x g at 30 °C for 30 min. After spinning, 2 ml of cancer cell medium were added and cells were incubated overnight. The next day, medium got exchanged. Another 24 h later, puromycin (final concentration: 2,5 µg/ml) was added to select the plasmid-containing cells. Non-infected cells served as a control. Selection with puromycin was carried out until all control cells had died (6-8 d).

7.2.5 Calculation of the CAS9 efficiencies

To calculate the CAS9 efficiency, the protocol from (Brinkman, Chen et al. 2014) was used. Therefore, transfected cells using PTEN sgRNA 1, sgRNA 4, lac-z sgRNA or non targeting

sgRNA were harvested, and the DNA was purified with mammalian DNA elute kits from SIGMA. Then, a PCR (**Table 17, 18**) was performed to amplify the gene section of interest. Following, the PCR product was purified using the NEB PCR purification kit and afterwards the purified PCR product was sent for sequencing. With the TIDE (tracking of indels by decomposition) online tool, two sequencing files were compared and the spectrum of indels was reconstructed (**Figure 7**). One file served as a control (non targeting or lac-z) and the second file contained the edited sequence (PTEN_1 or PTEN_4). The CAS9 editing efficiency then was calculated by subtracting the amount of indels with a length of 0 bp from 100%. The CAS9 efficiencies of both cell lines used are listed in **Table 20**.

7.3 Molecular biology

7.3.1 Isolation of DNA

Cultured cells were washed with PBS and scraped off the plate when confluent. The PBS-cell suspension was centrifuged (1000 rpm, 5 min) before discarding the supernatant fluid. Mammalian DNA elute kits from SIGMA (GenELUTE™) then were used to extract DNA from the remaining cell pellet. To purify PCR products, purification kits from NEB were used. For genotyping PCRs cells were washed one time in PBS and lysed with 50 µl of vor Soriano lysis buffer, containing phosphatase inhibitor and DTT. Lysis was performed in a thermocycler set to the following conditions:

99°C	Preheating
55°C	90 min
95°C	15 min
25°C	Pause

Table 15. Thermocycler program for cell lysis

7.3.2 Polymerase chain reaction (PCR)

For the *Pdk1* recombination PCR (*Pdk1*-del) (Table 16) and the TIDE analysis PCRs (Table 17, 18), a pre-mix containing taq-polymerase, buffer and dNTPs was used.

Reagent	Amount (µl)
Pre-mix	12,5
Pdk1-i4-UP2	0,4
Pdk1 del UP	1
Pdk1 LP	0,6
H_20	9,5

Conditions		
95°C	3 min	
95°C	45 s	40x
63°C	1 min	
72°C	1 min 30 s	

Table 16. PCR-reaction mix and thermocycler program for the *Pdk1*-del PCR.

Reagent	Amount
Genomic DNA	50 ng
Pten_1 fw	2 µl (of 10 µM stock)
Pten_1 rev	2 µl (of 10 µM stock)
H_20	21 µl

Conditions		
95°C	1 min	
95°C	15 s	25x
53°C	1 min	
72°C	1 min	

Table 17. PCR-reaction mix and thermocycler program for the TIDE analysis PCR. The PCR product was used to check the efficiency of CAS9 editing using the Pten sgRNA 1.

Reagent	Amount
Genomic DNA	50 ng
Pten_4 fw	2 µl (of 10 µM stock)
Pten_4 rev	2 µl (of 10 µM stock)
H_20	21 µl

Conditions		
95°C	1 min	
95°C	15 s	25x
54°C	1 min	
72°C	1 min	

Table 18. PCR-reaction mix and thermocycler program for the TIDE analysis PCR. The PCR product was used to check the efficiency of CAS9 editing using the Pten sgRNA 4.

7.3.3 Separation of DNA by agarose gel electrophoresis

DNA was separated on 2% agarose gels. The agarose was dissolved using 1x TAE buffer and a microwave to boil the mixture. Before pouring it into the cast, ethidiumbromide was added to the gel. DNA samples were pipetted into the gel wells and separated at 120 V. Results were documented after UV-light excitation (UVP UVsolo *touch*).

7.4 Protein biochemistry

7.4.1 Protein extraction

For protein harvesting, cells were seeded in culture dishes. When the cells were 70-80% confluent, the medium was discarded and the cells were washed two times with ice-cold PBS. Then, a mixture of 150 µl IP-lysis buffer supplemented with protease inhibitor and phosphatase inhibitor were added. The cells were detached from the plate with a plastic scraping tool and collected in Eppendorf tubes before freezing them in liquid nitrogen. When frozen, the samples were stored at -80 °C.

7.4.2 Protein quantification

Bradford assay (Bradford 1976) was used to estimate the protein concentration of the samples. Therefore, 300 µl of a 1:5 Bradford reagent:water dilution was pipetted into each well of a 96-well plate before 1 µl of the sample was added. After incubation for 10 minutes, absorbance was measured at 595 nm. For each sample the measurement was performed in triplicates. The protein concentration was estimated based on a BSA standard curve. By adding IP lysis buffer and 5x Laemmli buffer, the protein concentration of the lysates were equalized. The samples were then heated to 95 °C for 5 minutes before storing at -80 °C or performing SDS-PAGE.

7.4.3 SDS polyacrylic gel electrophoresis (SDS PAGE)

To separate proteins according to their molecular weight, SDS PAGE was performed. First, the reagents for the 10% separating gel (**Table 19**) were mixed with a vortex mixer before poured into a cast and weighted with isopropanol until polymerized. Isopropanol was removed and stacking gel (**Table 19**) was poured into the cast and a comb was placed. After

Stacking gel (1x)		Separating gel (1x)	
ddH_2O	1500 µl	ddH_2O	2050 µl
Stacking gel buffer	650 µl	Separating gel buffer	1300 µl
30% acrylamide	375 µl	30% acrylamide	1650 µl
10% SDS	25 µl	10% SDS	50 µl
10% APS	12.5 µl	10% APS	25 µl
TEMED	5 µl	TEMED	7.5 µl

Table 19. Stacking and separating gel recipes for SDS-PAGE.

polymerization of the stacking gel, the comb was removed and the samples were added to the wells. Broad range protein ladder from Thermo Scientific ™ was used as a reference. Voltage was set to 80 mV. When the loading reached the end of the stacking gel, proteins were separated by setting voltage to 100 mV.

7.4.4 Immunoblotting

After SDS PAGE, proteins were blotted onto a nitrocellulose membrane. Therefore, the gel with separated proteins and the nitrocellulose membrane were placed into a bracket as shown in **Figure 6**. The sandwich was placed in a tank containing transfer buffer. Proteins were transferred at 300 mA for 2 hours before blocking the membrane in 5% milk (95% TBS-0.1% TWEEN) for one hour. Next, the membrane was incubated with a specific antibody solution in 5% milk-TBS-1%Tween overnight at 4 °C. The next day, the primary antibody solution was removed, and the membrane was washed for 15 min with TBS-0.1% Tween. After two more identical washing steps, the secondary antibody in 5% milk (95% TBS-0.1% TWEEN) was added to the membrane, incubating one hour at room temperature in the dark before washing the membrane again three times with TBS-1%Tween. Then, the membrane was scanned at 600 or 800 nm in an Odyssey® imaging system.

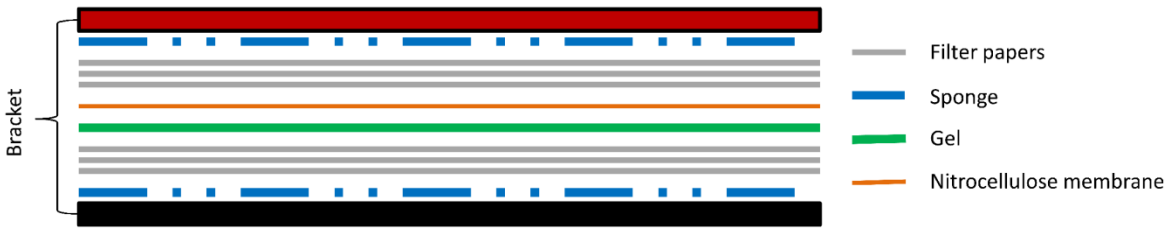

Figure 6. Scheme of the immunoblot „sandwich“

7.6 Statistical analysis

Statistical analysis, graph design and data correlation were performed with GraphPad Prism 5. The obtained data was plotted as mean values ± standard deviation. The Clonogenic assays were performed in triplicates, CellTiterGlo® assays in quadruplicates. For the calculation of statistical significance in the clonogenic assays, unpaired t-tests were applied. For statistical analysis of CellTiterGlo® assays, raw data was normalized and two-way analysis of variance (ANOVA) was performed. Results with $p<0.05$ were considered as statistically significant.

8. Results

8.1 *Pdk1* deletion impairing PDAC growth in vitro

Blocking of PI3K/PDK1 signaling impairs PDAC formation and plasticity in vivo. (Eser, Reiff et al. 2013) To investigate the impact of *Pdk1* deletion in vitro, murine *Pdx1-Flp;FSF-Kras*$^{G12D/+}$;*FSF-R26*$^{CAG\text{-}CreERT2}$;*Pdk1*$^{lox/lox}$ PDAC cells were used. The cells were treated for 8 days with 4-OHT before performing a cell viability assay (CellTiter Glo®). The CellTiter-Glo® reagent results in cell lysis and generates a luminescent signal proportional to the cellular ATP level, which can be used to measure cell viability. For this experiment 500 with EtOH or 4-OHT treated cells (CV7250) were seeded per well (96-well plate) as quadruplicates. At five time points (day 0 - day 4) CellTiter Glo® reagent was added and luminescence was measured.

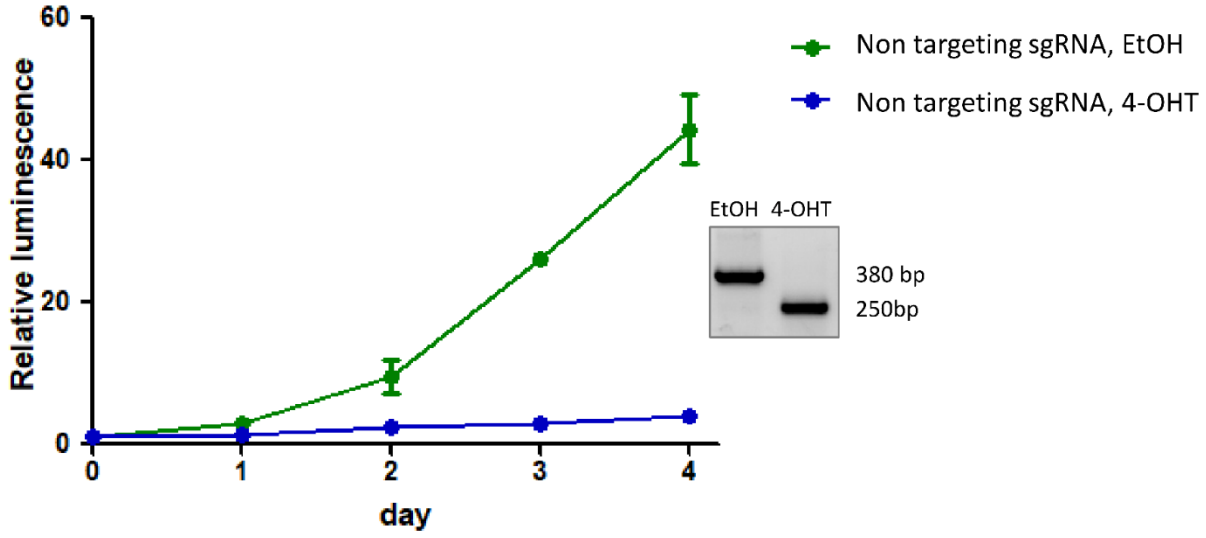

Figure 7. *Pdk1*-deletion impairs growth of PDAC cells in vitro
4-OHT-treated cells get arrested in growth, while the EtOH-treated control cells proliferate. Cells were treated for 8 d with 4-OHT or EtOH for this assay.

Previously, a genome-wide KO enrichment screen was used to screen for genes, whose KO results in a resistance to *Pdk1*-deletion. One of the main hit genes in this screen was *Pten*. This method is based on positive selection: in a pool of cells, every cell has a different gene deleted by CAS9. Therefore, a whole genome sgRNA library is necessary. Then, the gene of interest (*Pdk1*) gets deleted. The cells which gained resistance throughout the first deletion

will continue growing, while the rest of the cells get arrested in growth as they are dependent on *Pdk1*. Subsequent genome sequencing and analysis captures the counts of the previously used sgRNAs. The more enriched a sgRNA is, the more cells with the corresponding genetic mutation proliferated after *Pdk1*-deletion.

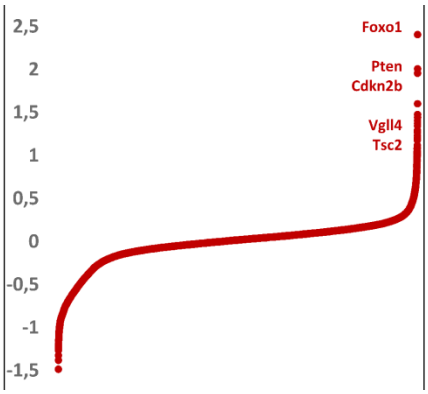

Figure 8. PTEN sgRNAs are enriched in genome wide KO screen
Deletion of the hit genes using the CAS9 endonuclease leads to a resistance against *Pdk1* deletion. Unpublished data by K. Sleiman, Saur lab.

8.2 Creating PTEN-KO cells

PTEN-KO cells were created using the CRISPR/CAS9 system and lentiviral transduction in order to validate *Pten*-loss as a putative resistance mechanism. The two most enriched sgRNAs from the previous CRISPR/CAS9 knockout enrichment screen in the Saur lab were chosen and a non targeting sgRNA as well as a lac-z sgRNA served as controls. The sequences of the sgRNAs used are listed in **Table 9**. **Figure 10** shows the CAS9 efficiencies in the *Pten* gene of the tested cell lines[2] and a protein immunoblot confirming PTEN-KO. **Figure 11** provides how the CAS9 efficiencies were calculated with TIDE. PTEN sgRNA1 and *Pten* sgRNA4 are abbreviated as PTEN_1 and PTEN_4 in the following.

[2] http://shinyapps.datacurators.nl/tide/ was used to calculate the Cas9 efficiencies

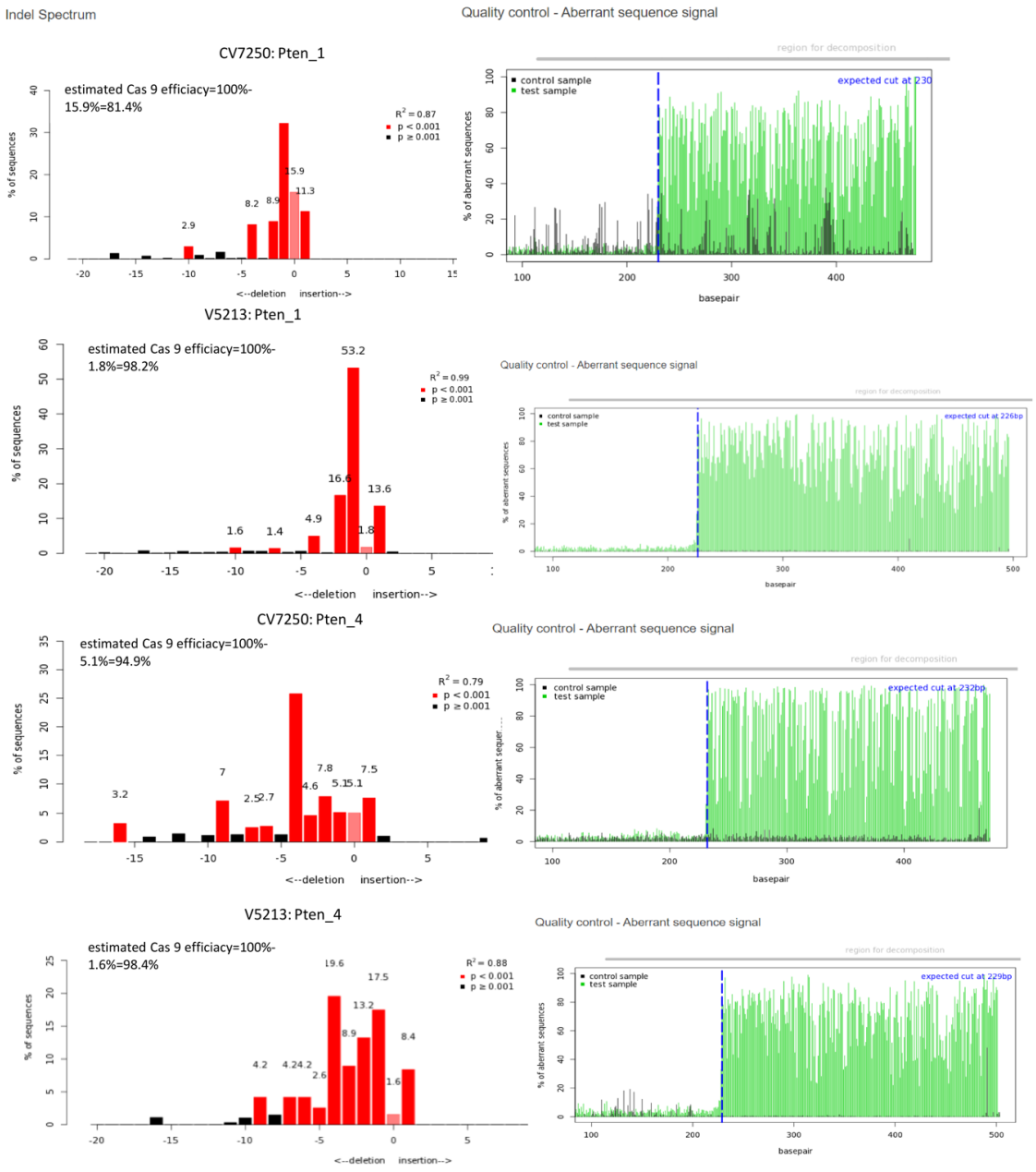

Figure 9. CAS9 efficiency can be calculated with TIDE online application

This example shows the calculations of the CAS9-cutting efficiency by the online tool TIDE. Because TIDE only calculates with indels up to 50 bp, the listed percentages in Table 1 were calculated by subtracting the amount of 0 bp from 100%. Thereby also possible indels with a length of more than 50 bp could be included. In this case the CAS9 efficiency would be assumed to be 100%-2.1%=97,9%.

	CV7250	V5213
PTEN sgRNA1	81.4%	98.2%
PTEN sgRNA4	94.9%	98.4%

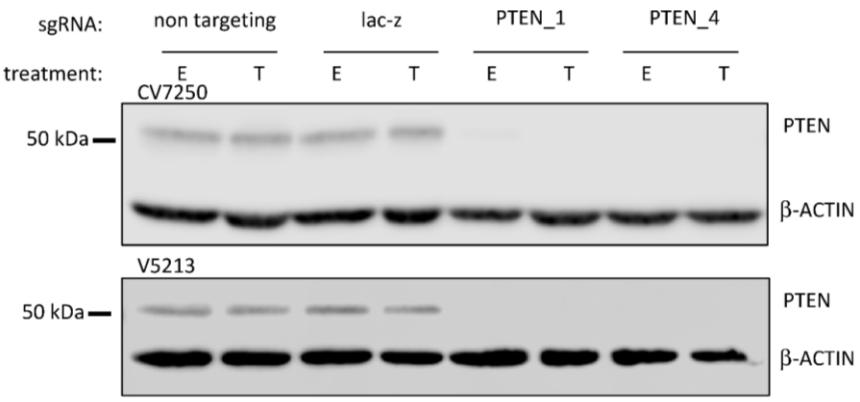

Figure 10. CAS9 enables KO of PTEN
Top, CAS9 efficiencies of the tested cell lines. Below, Protein immunoblot confirming PTEN-KO. The cells were treated with EtOH (E) or 4-OHT (T) before harvesting protein. β-ACTIN was used as a loading control.

8.3 PTEN deletion causing resistance to PDK1-loss

To investigate a possible resistance to *Pdk1* deletion, a suitable assay to visualize a rescue effect was necessary. A clonogenic assay using crystal violet staining was chosen to display the possible differences in growth between the control cells (lac-z, non targeting) and the PTEN-KO cells. This assay directly yields information about cell colony growth between two time points. The cells were treated for 8 days with EtOH as a control, or with 4-OHT to delete *Pdk1*. PCR and agarose gel electrophoresis were conducted to check the recombination status of the cells. The recombined variant showed a 250 bp band, whereas the wild type variant (EtOH-treated) showed a 380 bp band (**Figure 12 C, H***)*. Furthermore, protein immunoblot analysis showed a full deletion of *Pdk1* after 4-OHT treatment (**Figure 12 E, J**). For the clonogenic assay, 2000 cells were seeded per well using 6-well plates. The plates were incubated for 10 respectively 15 days before staining the cells with crystal violet. After staining the wells containing the 4-OHT treated cells were compared. In the plates seeded

with PTEN-KO cells, a higher count was recorded and bigger colonies were observed in comparison to the lac-z and non targeting control, an effect visible in both tested cell lines (**Figure 12 A, F**). To test significance and to quantify the rescue effect induced by PTEN deletion, the crystal violet stainings were solubilized with 1% SDS solution; absorbance was then measured at 570 nm (**Figure 12 B, D***).* PTEN-KO cells showed a significant rescue compared to the lac-z and non targeting controls. The clonogenic crystal violet assay offers direct information about cell growth but not about cell metabolism. An ATP based method provides even more information about cell viability and vitality. Therefore, CellTiter Glo® assay was performed on the CV7250 cell line. **Figure 12 K** shows the mean values of the 4-OHT treated cells normalized to day 0. The PTEN-KO cells showed significantly higher values than the lac-z and non targeting controls. In summary, PTEN-KO led to significant resistance to *Pdk1* deletion without leading to a complete rescue of the cells, as the EtOH controls showed a higher proliferation than the PDK1/PTEN-KO cells (**Figure 12 A, F**).

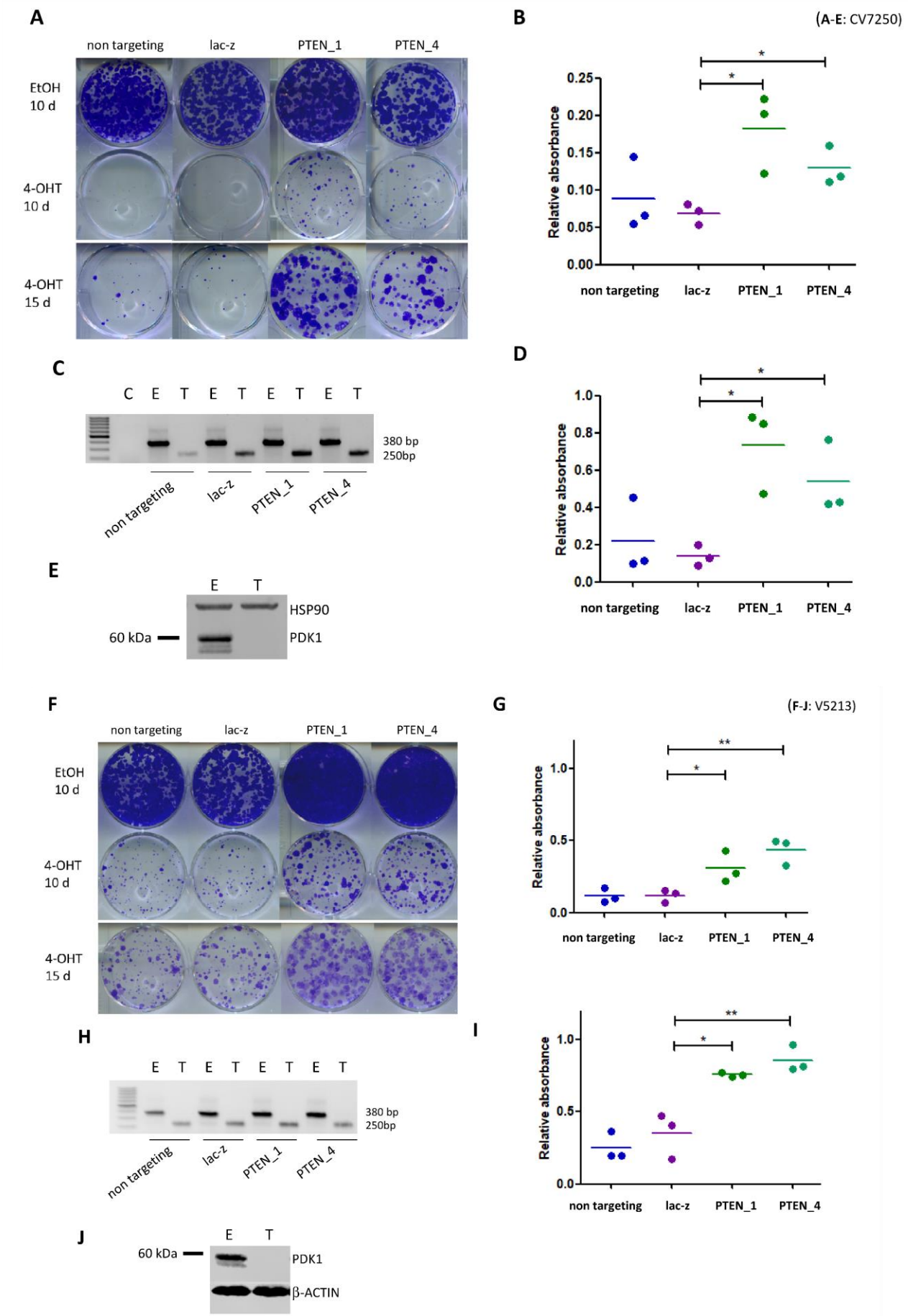
A
non targeting
lac-z
PTEN_1
PTEN_4
EtOH
10 d
4-OHT
10 d
4-OHT
15 d
B
(A-E: CV7250)
Relative absorbance
0.25
0.20
0.15
0.10
0.05
0.00
*
*
non targeting
lac-z
PTEN_1
PTEN_4
C
C E T E T E T E T
380 bp
250bp
non targeting
lac-z
PTEN_1
PTEN_4
D
Relative absorbance
1.0
0.8
0.6
0.4
0.2
0.0
*
*
non targeting
lac-z
PTEN_1
PTEN_4
E
E T
HSP90
60 kDa
PDK1
F
non targeting
lac-z
PTEN_1
PTEN_4
EtOH
10 d
4-OHT
10 d
4-OHT
15 d
G
(F-J: V5213)
Relative absorbance
1.0
0.5
0.0
**
*
non targeting
lac-z
PTEN_1
PTEN_4
H
E T E T E T E T
380 bp
250bp
non targeting
lac-z
PTEN_1
PTEN_4
I
Relative absorbance
1.0
0.5
0.0
**
*
non targeting
lac-z
PTEN_1
PTEN_4
J
E T
60 kDa
PDK1
β-ACTIN

K

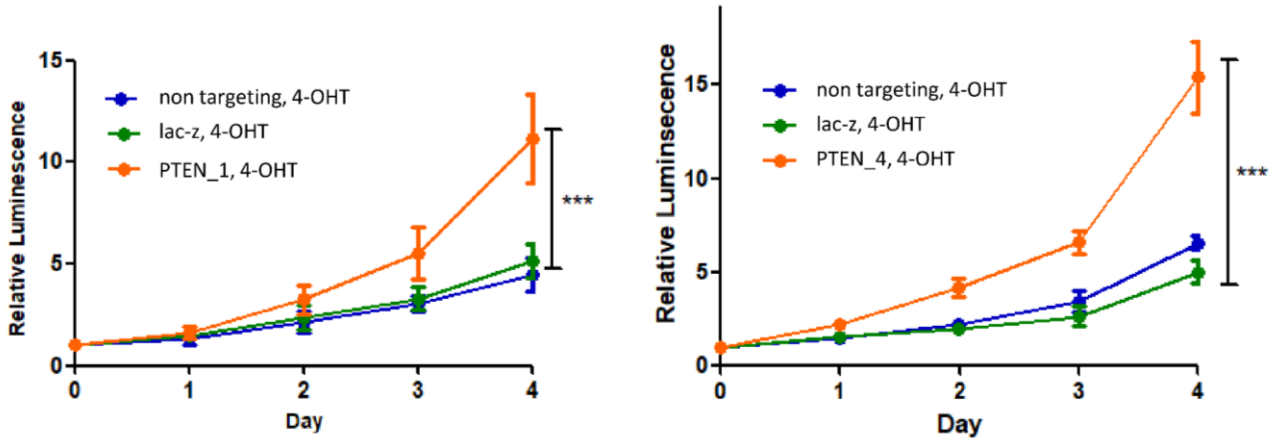

Figure 11. PTEN-KO causes in vitro resistance to deletion of *Pdk1*

A: Clonogenic assay with cell line CV7250. Crystal violet-stained plates after 10 and 15 days (10 d, 15 d) of incubation. A representative replicate out of three replicates shown.

B: Absorbance values at 570 nm of the solubilized plates from **A** (4-OHT-treated, 10 d incubation). Data showing mean values of all replicates; n=3 replicates; *p<0.05; unpaired t-test.

C: Gel electrophoresis of cells from the CV7250 line showing the recombination status after treatment with EtOH (E) or 4-OHT (T).

D: Absorbance values at 570 nm of the solubilized plates from **A** (4-OHT-treated, 15 d incubation). Data showing mean values of all replicates; n=3 replicates; *p<0.05; unpaired t-test.

E: Immunoblot analysis of PDK1 in CV7250-cells after 4-OHT (T) or EtOH (E) treatment.

F: Clonogenic assay with cell line V5213. A representative replicate out of three replicates shown.

G: Absorbance values at 570 nm of the solubilized plates from **F** (4-OHT-treated, 10 d incubation) Data showing mean values of all replicates; n=3 replicates; **p<0.01; *p<0.05; unpaired t- test.

H: Gel electrophoresis of cells from the V5213 line, showing the recombination status after treatment with EtOH (E) or 4-OHT (T).

I: Absorbance values at 570 nm of the solubilized plates from **F** (4-OHT-treated, 15 d incubation). Data showing mean values of all replicates; n=3 replicates; **p<0.01; *p<0.05; unpaired t- test.

J: Immunoblot analysis of Pdk1 in V5213-cells after 4-OHT (T) or EtOH (E) treatment.

K: ATP based assay (CellTiter Glo®) comparing 4-OHT treated PTEN-KO cells with lac-z/non targeting controls. Data shown as mean +/- SD; normalized to D=0; left: n= 3 replicates, ***p<0.0001; two-way ANOVA, right: n=1 replicate ***p<0.0001; two-way ANOVA

8.4 Cell cycle arrest after *Pdk1* deletion is bypassed by PTEN-KO

The previous assays showed that PTEN-KO significantly lead to a rescue of *Pdk1* deletion. To investigate the mechanism of the growth arrest induced by *Pdk1* deletion, a cell cycle assay was performed. This experiment uses flow cytometry to measure DNA content in the respective cell groups, which allows the classification of a cell-fraction into a specific phase of the cell cycle. In the cell cycle, two stages can be differentiated; the mitosis (M) as a process of cellular division and the interphase as the intermediate part between two M phases. The interphase encloses the synthesis (S) phase in which DNA replication occurs. A gap (G1) precedes the S phase and another gap (G2) follows it. In G1 the cell prepares for DNA synthesis, in G2 for mitosis. After G1, the cell can go into a resting phase (G0) instead of entering S phase (**Figure 13**) (Vermeulen and Dirk 2003).

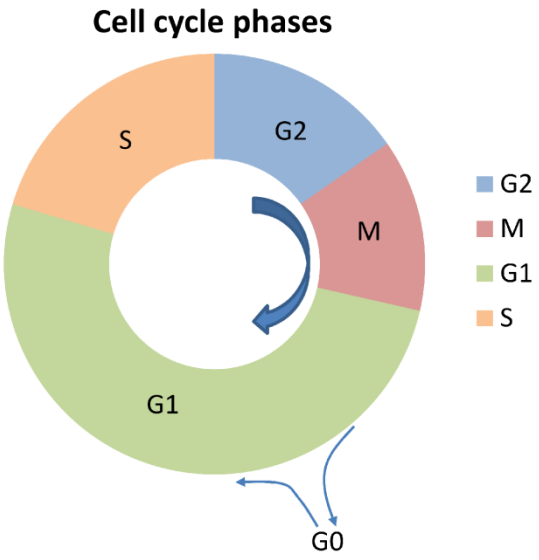

Figure 12. Scheme of cell cycle phases
The cell cycle can be divided into the mitosis (M) and interphase (G1, S, G2).

The cell cycle assay differentiates which fraction of cells already replicated the DNA in the S phase. These cells contain the doubled amount of DNA than the cells which have not completed DNA replication. The flow cytometry measures the amount of DNA and enables cell cycle-phase specific classification into the G0/G1 or G2/M fraction. For the assay, EtOH- or 4-OHT-treated cells were stained with propiumiodide (PI) to stain the DNA before carrying out flow cytometry. The protocol for this experiment was used from Hassan, Schneeweis et

al. 2018. The experiment showed that *Pdk1* deletion in the lac-z control cells led to a higher amount of cells in the G0/G1 fraction, which can be interpreted as an arrest in the G0 or G1 phase. This result is consistent with previous findings (Nakamura, Sakaue et al. 2008). Also a lower amount of cells in the G2/M fraction was visible, which can be interpreted as a decreased transition to the G2 or M phase (**Figure 14**). This cell cycle arrest seemed to be bypassed in the PTEN-KO cells. Here, the amount of cells in the G2/M fraction decreased only minimally after 4-OHT treatment.

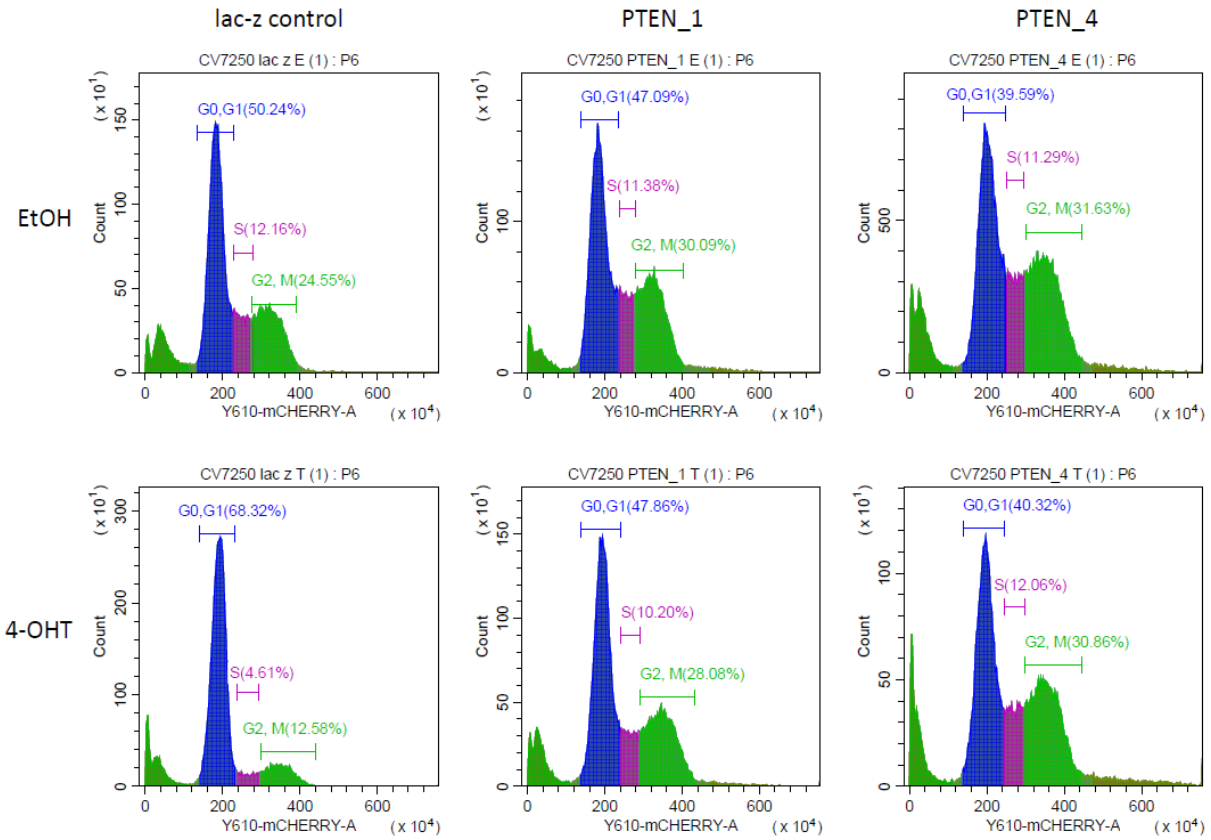

Figure 13. Cell cycle arrest after *Pdk1*-deletion is bypassed by PTEN-KO

Cell cycle analysis of CV7250 lac-z control cells and PTEN-KO (Pten_1, Pten_4) cells after 8 d treatment with EtOH or 4-OHT. A representative replicate out of three replicates shown.

8.5 PTEN-KO leads to upregulation of phosphorylated AKT (p-AKT)

Protein immunoblotting (**Figure 15**) showed that phosphorylation sites of AKT, S473 and T304, are up regulated in the EtOH treated PTEN-KO cells. In the non targeting and lac-z control cells, p-AKT was not detectable using western blot, presumably due to low protein concentrations. The 4-OHT treated PTEN-KO cells showed a decreased p-AKT (T308) protein level. In contrast, the p-AKT (S473) level was stable after *Pdk1* deletion. This led to the question if AKT is active with only one site phosphorylated, so the downstream targets S6 and FOXO1 were analyzed.

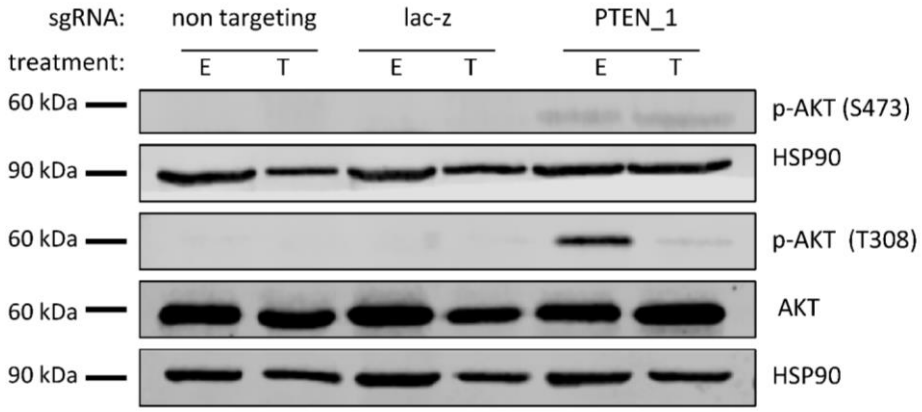

	non targeting		lac-z		PTEN_1	
	E	T	E	T	E	T
p-AKT S473	0.005	0.209	0.050	0.088	0.697	0.949
p-AKT T308	0.069	0.0837	0.127	0.067	4.13	0.314

Figure 14. PTEN-KO increases amount of p-AKT
Protein immunoblot comparing non targeting and lac-z control cells with Pten-KO cells. Cells were treated with EtOH (E) or 4-OHT (T) for 8 days before harvesting protein. HSP90 served as a loading control. The table below shows signal intensity values of the p-AKT T308/S473 immunoblot.

Protein immunoblotting (**Figure 16**) showed higher levels of phosphorylated S6 (S235-236) in the EtOH treated PTEN-KO cells, but not in the 4-OHT treated cells. In addition, the amount of phosphorylated FOXO1 (T24, S319) is increased in the PTEN-KO cells compared to the controls (non targeting, lac-z). SGK1, which contributes to the phosphorylation FOXO1 T24 and S319 (Hedrick, Hess Michelini et al. 2012) was stable at all conditions. Expression of Cyclin D1 was found to be slightly decreased in the PDK1-deficient cells. Because p-AKT S473

is phosphorylated by mTORC2 (Emmanouilidi, Fyffe et al. 2019), protein levels of mTOR as well as p-mTOR serine 2481 (S2481) and serine 2448 (S2448) were tested via protein immunoblotting (**Figure 17**). S2481 and S2448 are phosphorylated upon activation of mTORC2, making them potential markers for mTORC2 activity (Copp, Manning et al. 2009). Control cells (non targeting, lac-z) and PTEN-KO cells showed higher mTOR amounts after 4-OHT-treatment whereby the upregulation in the PTEN-KO seemed more prominent. The amount of p-mTOR S2481 also increased after *Pdk1* deletion, but PTEN-KO cells showed slightly lower amounts than the control cells. Also, p-mTOR S2448 levels increased after 4-OHT treatment. The amounts in the EtOH-treated cells seemed to be higher in the non targeting and lac-z controls. Protein amounts of RICTOR, which is part of mTORC2, were consistent in the lac-z and non targeting control cells. In the PTEN-KOs EtOH treated cells showed a lower mTOR level than the 4-OHT treated cells. Phosphorylated RICTOR (T1135), which is known to be induced by oncogenic RAS and PI3K (Boulbes, Chen et al. 2010), only was detectable in the EtOH controls and showed no band after *Pdk1* deletion.

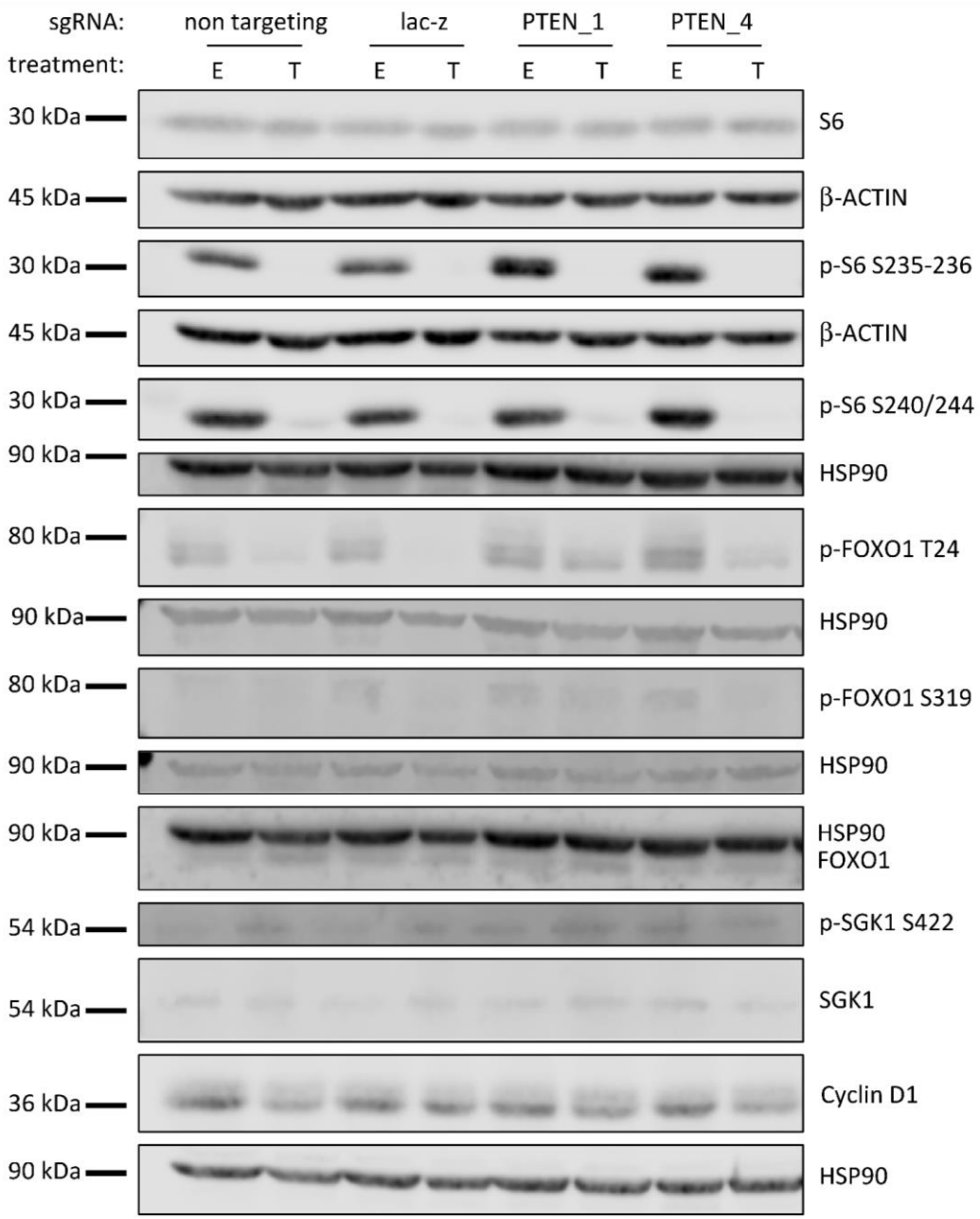

Figure 15. PDK1-KO alters PI3K/AKT signaling

Protein immunoblot comparing protein levels of control (non targeting, lac-z) and PTEN-KO cells (PTEN_1, PTEN_4). Cells were treated with EtOH (E) or 4-OHT (T) for 8 days before harvesting protein. HSP90 and β-ACTIN functioned as loading controls.

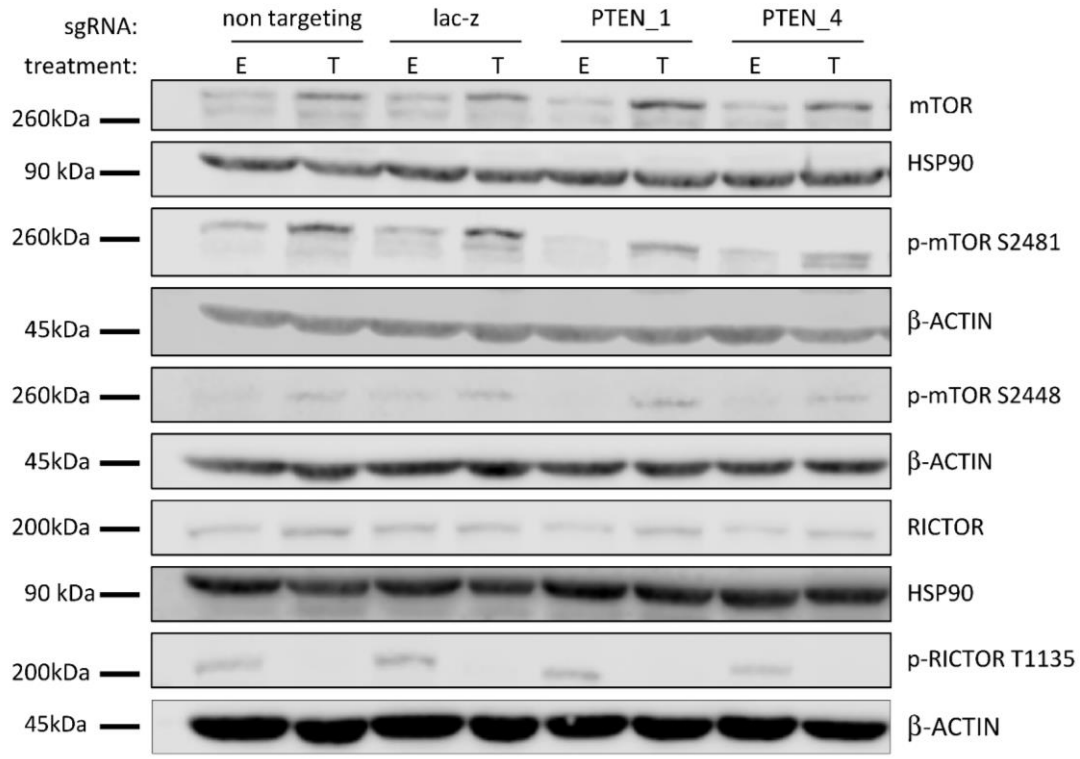

Figure 16. PDK1 deletion increases mTOR amount

Protein immunoblot comparing protein levels of control (non targeting, lac-z) and PTEN-KO cells (PTEN_1, PTEN_4). Cells were treated with EtOH (E) or 4-OHT (T) for 8 days before harvesting protein. HSP90 and β-ACTIN functioned as a loading control.

9. Discussion and outlook

PDK1 has been shown to be essential for KRAS-driven PDAC initiation and progression, which makes it an attractive possible target protein for researchers in the field of pancreatic cancer (Eser, Reiff et al. 2013, Schonhuber, Seidler et al. 2014). In this dissertation it was shown that deletion of the protein PTEN induces a significant resistance in PDK1-deficient PDAC cells. Furthermore, signaling pathway alterations in the PI3K/AKT axis were found in PTEN-KO cells, which may play a role in the resistance mechanism. The data presented in this thesis could contribute to the laborious process of finding genotype-specific therapeutic approaches in future PDAC treatments.

9.1 PTEN-KO PDAC cells show resistance against *Pdk1* deletion

To see the effects of a PTEN deletion on growth of PDJ1-deficient cells, PTEN-KO cells had to be created. Using the CRISPR/CAS9 technique, CAS9 efficiencies from 81.4% - 98.4% (**Figure 10**) were archived. These numbers were calculated with the online tool "TIDE" and describe the amount of small insertions or deletions (up to 50 bp) in the DNA in a pool of cells. Protein immunoblotting confirmed PTEN-KO, no band could be detected in the respective samples (**Figure 11**). The *Cre*^{ER}-*loxP* system in the used cell lines allowed us to delete *Pdk1* by treating the cells with 4-OHT for 8 days. Corresponding control cells were treated in the same way with EtOH. The *Pdk1* deletion was confirmed via PCR and protein immunoblotting (**Figure 12 E, J**). The cells were then seeded for a clonogenic assay to detect differences in growth between the PDK1-deficient cell groups (**Figure 12 A, B, D, F, G, I**). The control cells (lac-z sgRNA, non targeting sgRNA) formed less and smaller colonies than the PTEN-KO cells. This effect was visible after 10 days, and the difference even increased after 15 days which indicates a growth advantage for the PTEN-KO cells. To quantify these results, the staining of the cells was solubilized with 1% SDS and the absorbance was measured at 570 nm. The absorbance values of the plates containing PTEN-KO cells were significantly higher than the corresponding lac-z and non targeting controls. It is important to mention that this rescue effect did not reach the growth level of the EtOH control cells. A residual amount of active PTEN in the PTEN-KO cells was excluded via protein immunoblotting (**Figure 11**). The online

tool TIDE calculated CAS9 efficiencies for the PTEN-KO cells from 81.4%-98.4%. This tool only considers indels up to 50 bp. The fact that no PTEN band could be shown in the western blot could be explained by indels bigger than 50 bp or by very low PTEN protein concentrations. In the ATP-based CellTiter Glo® assay, PDK1-deficient PTEN-KO cells also showed higher luminescence values than non targeting or lac-z controls. These results indicate that not only cell growth and cell number is increased, but also cells show significant resistance from a metabolic point of view as this assay is ATP-level based. To further circumscribe the resistance mechanism against PDK1-loss, cell cycle assays were performed. This assay uses flow cytometry to measure the DNA amount in the cells, allowing to assign them into cell cycle phase-specific fractions (**Figure 14**). In the lac-z control cells, *Pdk1* deletion led to a G2-block and a higher G0/G1 fraction. This finding is consistent with a study from Nakamura, Sakaue et al. (2008) in which PDK1-KO cells showed a delayed transition from G0/G1 to S phase. A decreased level of Cyclin D1 was associated with the inhibited cell cycle progression in this study. The proto-oncogene Cyclin D1 is an important regulator in the cell cycle, promoting the progression from the G1 to S phase (Alao 2007). In our experiment only slightly decreased Cyclin D1 levels in *Pdk1* deleted cells were detected (**Figure 16**). PTEN-KO cells showed almost no cell cycle inhibition after *Pdk1* was deleted. This indicates a mechanism enabling the bypass of cell cycle respective functions of PDK1, independently of Cyclin D1 expression.

9.2 PTEN-KO leads to upregulated p-AKT

As described in the introduction of this thesis, phosphorylation at threonine 308 (T308) and serine 473 (S473) leads to full AKT activation. PDK1 is known to phosphorylate AKT at T308 (**Figure 18**). Protein immunoblotting showed an up regulation of p-AKT T308 in PTEN-KO cells (**Figure 15**). A possible explanation for this result could be the following: Because PTEN dephosphorylates PIP_3 to PIP_2, a lower PTEN level consequently leads to a higher level of PIP_3 and thus to a more sufficient recruitment of AKT and PDK1 to the cellular membrane, resulting in higher amount of p-AKT T308. After *Pdk1* deletion the p-AKT T308 band appeared much weaker, emphasizing the dependency of this phosphorylation site on Pdk1. The non targeting and lac-z control cells showed no p-AKT T308 band, which might be

explained by much lower protein levels. The second phosphorylation of AKT (S473) is catalyzed by mTORC2 which normally leads to fully activated AKT. THE KO of PTEN also led to up regulated amounts of this phosphorylation. In contrast to T308, the S473 phosphorylation was stable due to deletion of *Pdk1*. This could indicate an upregulated activity of mTORC2 in PDK1-deficient PTEN-KO cells. Similar data is presented in a study of Zhao, Lu et al. (2014) where PDK1-deficient mice developed heart failure, which was reversed after PTEN-KO. Their work showed that increased AKT activity was responsible for the cardiac protection in PDK1-deficient mice. This leads to the question if AKT is still active with only the S473 site phosphorylated.

To test this hypothesis, two downstream targets of AKT, S6 and FOXO1 (**Figure 18**), were

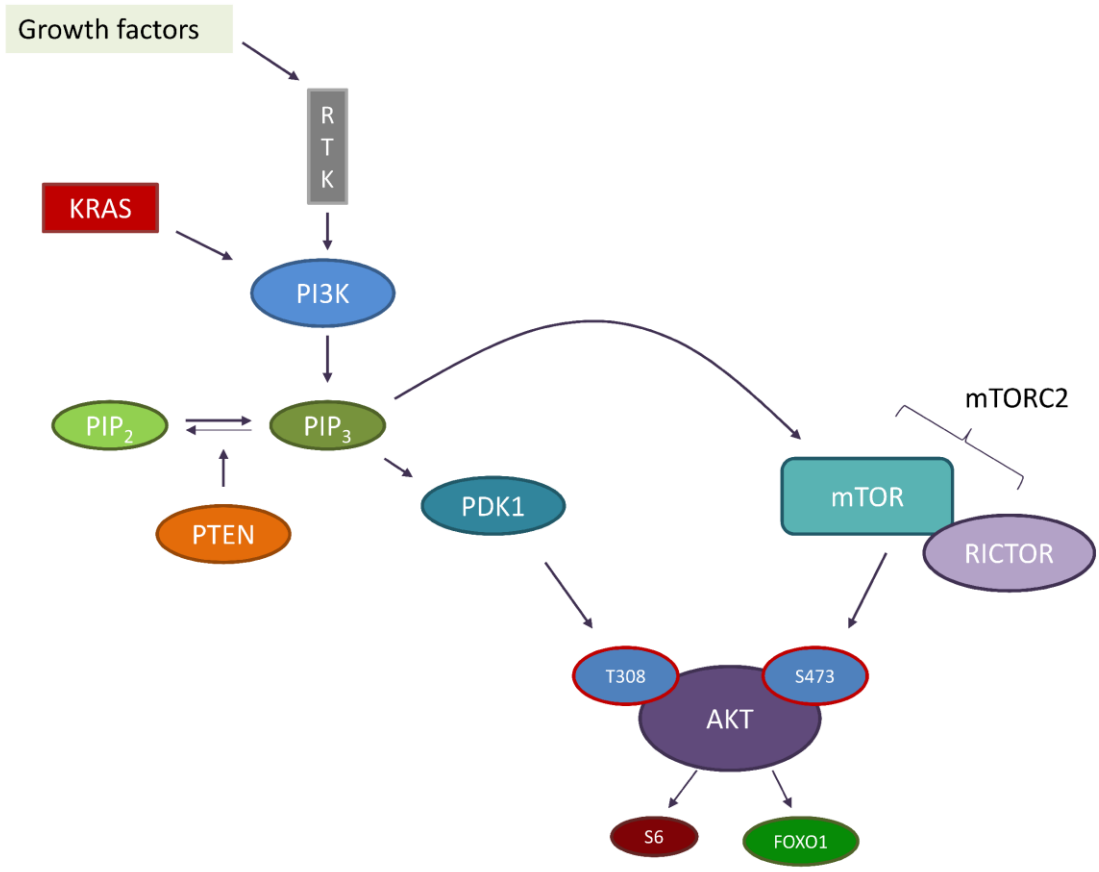

Figure 17. Downstream KRAS, PI3K/PDK1/AKT signaling involves mTORC2
Growth factors stimulate receptor tyrosine kinases (RKT) leading to an activation of PI3K. Through catalytic activity of activated PDK1 and mTORC2, AKT is phosphorylated at T308 and S473. This leads to an activation of AKT promoting cell growth, proliferation and survival.

analyzed (**Figure 16**). P-S6 serine 235-236 (S235-236) and p-S6 serine 240/244 (S240/244) showed almost no bands after *Pdk1* deletion. In contrast, the EtOH control cells showed p-S6 bands. These bands were visibly more prominent in the PTEN-KO cells. These findings punctuate the dependency of these phosphorylation sites on PDK1 but do not indicate active Akt in the 4-OHT treated PTEN-KO cells.

The p-FOXO1 sites threonine 24 (T24) and serine 319 (S319) are known to be downstream targets of AKT or SGK1. (Hedrick, Hess Michelini et al. 2012) Both, T24 and S319 showed a PDK1 dependency in the non targeting and lac-z control cells as almost no bands were detectable after 4-OHT-treatment. In the PTEN-KO cells, FOXO1 T24 and S319 levels were upregulated compared to the EtOH-treated control cells, somehow overcoming the PDK1 dependency. Interestingly, p-SGK1 S422 levels also were up regulated in the PTEN-KOs. This might contribute to the upregulated p-FOXO1 sites, as SGK1 contributes to the FOXO1-phosphorylation (Hedrick, Hess Michelini et al. 2012). FOXO transcription factors are known to be degraded after being phosphorylated at T24, S256 and S319 (Hedrick, Hess Michelini et al. 2012). The normal functions of FOXOs as triggering apoptotic responses or inducing cell cycle arrest are thereby inhibited (Schmidt, Fernandez de Mattos et al. 2002). Our results indicate that resistance of PTEN-KO cells to *Pdk1* deletion may be explained by a rescue of the PI3K/AKT signaling pathway, possibly due to an increased catalytic activity of AKT after PTEN-KO. This hypothesis is supported by the upregulated p-FOXO1 sites T24 and S319. However, an upregulated p-S6 level could not be detected in the PDK1-deficient PTEN-KO cells. This finding opposes this hypothesis, because S6 is a well characterized downstream target of AKT (Wittenberg, Azar et al. 2016).

9.3 *Pdk1* deletion leads to mTOR upregulation

As discussed before we showed that PTEN-KO lead to an upregulation of p-AKT S473 independently of PDK1 (**Figure 15**). This phosphorylation is catalyzed by mTORC2, so mTOR levels were tested. We showed that mTOR levels were increased after *Pdk1* deletion. This upregulation was stronger in the PTEN-KO cells than in the non targeting and lac-z controls. However, this result for itself does not prove higher mTORC2 levels because the used antibody is not specific for complex 2, but it is also sensitive for mTORC1. RICTOR which is

part of mTORC2 showed a slightly more prominent band in the PTEN-KO but not in the non targeting or lac-z control cells after *Pdk1* deletion (**Figure 17**). Combined with the higher mTOR levels, these results may be evidence for up regulated mTORC2 activity in PDK1-deficient cells caused by PTEN deletion. Zhao, Lu et al. (2014) also demonstrated in PDK1-PTEN-deficient mice that upregulated mTORC2 enhanced p-AKT S473 phosphorylation and thus led to higher AKT activity. This activation of AKT resulted in cardiac protection of mice and reversed heart failure, which had been developed after PDK1-KO. In contrast, they showed that removal of RICTOR diminished AKT S473 phosphorylation.

It has also been demonstrated that PIP_3 can directly increase mTORC2 activity (**Figure 18**) (Gan, Wang et al. 2011). In PTEN-KO cells PIP_3 levels could be increased as it would accumulate without being dephosphorylated to PIP_2 by PTEN.

To prove that mTORC2 is the factor enabling PDK1-independency, further experiments like treating PDK1-deficient PTEN-KO cells with mTORC2-inhibitors would be useful. This way, a possible resensitization of cells could be detected. If this mechanism can be validated in the future, PDAC patients with loss-of-function mutations of PTEN could possibly be treated with a combination of PDK1- and mTORC2-inhibitors. An experiment with a similar approach was performed in a study from Lynch, Polanska et al. (2018). They showed that a combined treatment with PI3K and mTOR inhibitors suppressed tumor growth in PTEN-KO cell lines.

9.4 Conclusion

To summarize, this thesis validated PTEN-loss by in vitro experiments as a mechanism to overcome *Pdk1* deletion induced growth arrest in PDAC. PDK1 is an attractive target protein for putative therapeutic approaches against pancreatic cancer, as it is required for PDAC initiation and progression. Clonogenic assays showed that PTEN-KO induces a resistance to PDK1-deficient cells and thereby leads to a significant rescue. The experiments in this work indicate that compensatory changes in the PI3K/AKT signaling pathway may be the cause for the resistance. To validate the molecular mechanistic behind the resistance, further experiments will be necessary.

10. Acknowledgements

I thank my supervisor Prof. Dr. Dieter Saur for letting me work at this interesting project, as well as PHD Candidate Katia Sleiman for introducing me into the lab and patiently giving me guidance through this project. I am grateful for the support of my brothers, especially Tobias for giving me his advice from the beginning of this work. Thanks to my parents Brigitte and Josef for constantly encouraging me and always lending a sympathetic ear. I am also very grateful to Jasmin for her love, patience and strong support even in stressful phases of this project.

11. References

Alao, J. P. (2007). "The regulation of cyclin D1 degradation: roles in cancer development and the potential for therapeutic invention." Molecular Cancer **6**(14): 1-16.

Alessi, D., M. Deak, A. Casamayor, F. Caudwell, N. Morrice, D. Norman, P. Gaffney, C. Reese, C. MacDougall, D. Harbison, A. Ashworth and M. Bownes (1997). "3-Phosphoinositide-dependent protein kinase-1 (PDK1):structural and functional homology with the DrosophilaDSTPK61 kinase." Current Biology **7**: 776-789.

Boulbes, D., C. H. Chen, T. Shaikenov, N. K. Agarwal, T. R. Peterson, T. A. Addona, H. Keshishian, S. A. Carr, M. A. Magnuson, D. M. Sabatini and D. Sarbassov dos (2010). "Rictor phosphorylation on the Thr-1135 site does not require mammalian target of rapamycin complex 2." Molecular Cancer Research **8**(6): 896-906.

Bradford, M. (1976). "A Rapid and Sensitive Method for the Quantitation ofMicrogram Quantities of Protein Utilizing thePrinciple of Protein-Dye Binding " Anlytical Biochemistry **72**: 248-254.

Bray, F., J. Ferlay, I. Soerjomataram, R. L. Siegel, L. A. Torre and A. Jemal (2018). "Global cancer statistics 2018: GLOBOCAN estimates of incidence and mortality worldwide for 36 cancers in 185 countries." CA Cancer Journal for Clinicians **68**(6): 394-424.

Brinkman, E. K., T. Chen, M. Amendola and B. van Steensel (2014). "Easy quantitative assessment of genome editing by sequence trace decomposition." Nucleic Acids Res **42**(22): e168.

Campbell, P. M., A. L. Groehler, K. M. Lee, M. M. Ouellette, V. Khazak and C. J. Der (2007). "K-Ras promotes growth transformation and invasion of immortalized human pancreatic cells by Raf and phosphatidylinositol 3-kinase signaling." Cancer Research **67**(5): 2098-2106.

Canley, L. (2002). "The Phosphoinositide 3-Kinase Pathway." Science **296**: 1655-1657.

Copp, J., G. Manning and T. Hunter (2009). "TORC-specific phosphorylation of mammalian target of rapamycin (mTOR): phospho-Ser2481 is a marker for intact mTOR signaling complex 2." Cancer Research **69**(5): 1821-1827.

Cox, A. D. and C. J. Der (2010). "Ras history: The saga continues." Small GTPases **1**(1): 1-27.

Cox, A. D., S. W. Fesik, A. C. Kimmelman, J. Luo and C. J. Der (2014). "Drugging the undruggable RAS: Mission possible?" Nat Rev Drug Discov **13**(11): 828-851.

Doench, J. G. (2018). "Am I ready for CRISPR? A user's guide to genetic screens." Nature Reviews Genetics **19**(2): 67-80.

Downward, J. (2008). "Targeting RAS and PI3K in lung cancer." Nature Medicine **14**(12): 1315-13166.

Emmanouilidi, A., C. A. Fyffe, R. Ferro, C. E. Edling, E. Capone, S. Sestito, S. Rapposelli, R. Lattanzio, S. Iacobelli, G. Sala, T. Maffucci and M. Falasca (2019). "Preclinical validation of 3-phosphoinositide-dependent protein kinase 1 inhibition in pancreatic cancer." Journal of Experimental Clinnical Cancer Research **38**(1): 1-12.

Engelman, J. A., J. Luo and L. C. Cantley (2006). "The evolution of phosphatidylinositol 3-kinases as regulators of growth and metabolism." Nature Reviews Genetics **7**(8): 606-619.

Eser, S., N. Reiff, M. Messer, B. Seidler, K. Gottschalk, M. Dobler, M. Hieber, A. Arbeiter, S. Klein, B. Kong, C. W. Michalski, A. M. Schlitter, I. Esposito, A. J. Kind, L. Rad, A. E. Schnieke, M. Baccarini, D. R. Alessi, R. Rad, R. M. Schmid, G. Schneider and D. Saur (2013). "Selective requirement of PI3K/PDK1 signaling for Kras oncogene-driven pancreatic cell plasticity and cancer." Cancer Cell **23**(3): 406-420.

Ferro, R. and M. Falasca (2014). "Emerging role of the KRAS-PDK1 axis in pancreatic cancer." World Journal of Gastroenterology **20**(31): 10752-10757.

Fruman, D. A. and C. Rommel (2014). "PI3K and cancer: lessons, challenges and opportunities." Natue Reviews Drug Discovery **13**(2): 140-156.

Gan, X., J. Wang, B. Su and D. Wu (2011). "Evidence for direct activation of mTORC2 kinase activity by phosphatidylinositol 3,4,5-trisphosphate." Journal of Biological Chemistry **286**(13): 10998-11002.

Gillen, S., T. Schuster, C. Meyer Zum Buschenfelde, H. Friess and J. Kleeff (2010). "Preoperative/neoadjuvant therapy in pancreatic cancer: a systematic review and meta-analysis of response and resection percentages." Plos Medicine **7**(4): 1-15.

Hassan, Z., C. Schneeweis, M. Wirth, C. Veltkamp, Z. Dantes, B. Feuerecker, G. O. Ceyhan, S. K. Knauer, W. Weichert, R. M. Schmid, R. Stauber, A. Arlt, O. H. Kramer, R. Rad, M. Reichert, D. Saur and G. Schneider (2018). "MTOR inhibitor-based combination therapies for pancreatic cancer." British Journal of Cancer **118**(3): 366-377.

Hedrick, S. M., R. Hess Michelini, A. L. Doedens, A. W. Goldrath and E. L. Stone (2012). "FOXO transcription factors throughout T cell biology." Nature Reviews Immunology **12**(9): 649-661.

Hill, R., J. H. Calvopina, C. Kim, Y. Wang, D. W. Dawson, T. R. Donahue, S. Dry and H. Wu (2010). "PTEN loss accelerates KrasG12D-induced pancreatic cancer development." Cancer Research **70**(18): 7114-71124.

Hopkins, B. D., C. Hodakoski, D. Barrows, S. M. Mense and R. E. Parsons (2014). "PTEN function: the long and the short of it." Trends Biochemical Science **39**(4): 183-190.

Jinek, M., K. Chylinski, I. Fonfara, M. Hauer, J. Doudna and E. Charpentier (2012). "A programmable dual RNA-guided DNA endonuclease in adaptive bacterial immunity." Science **337**: 816–821.

Kikani, C. K., L. Q. Dong and F. Liu (2005). ""New"-clear functions of PDK1: beyond a master kinase in the cytosol?" Journal of Cell Biochemistry **96**(6): 1157-1162.

Lynch, J. T., U. M. Polanska, U. Hancox, O. Delpuech, J. Maynard, C. Trigwell, C. Eberlein, C. Lenaghan, R. Polanski, A. Avivar-Valderas, M. Cumberbatch, T. Klinowska, S. E. Critchlow, F. Cruzalegui and S. T. Barry (2018). "Combined Inhibition of PI3Kbeta and mTOR Inhibits Growth of PTEN-null Tumors." Molecular Cancer Therapeutics **17**(11): 2309-2319.

Milella, M., I. Falcone, F. Conciatori, U. Cesta Incani, A. Del Curatolo, N. Inzerilli, C. M. Nuzzo, V. Vaccaro, S. Vari, F. Cognetti and L. Ciuffreda (2015). "PTEN: Multiple Functions in Human Malignant Tumors." Front Oncology **5**(24): 1-41.

Nakamura, K., H. Sakaue, A. Nishizawa, Y. Matsuki, H. Gomi, E. Watanabe, R. Hiramatsua, M. Tamamori-Adachi, S. Kitajima, T. Noda, W. Ogawa and M. Kasuga (2008). "PDK1 regulates cell proliferation and cell cycle progression through control of cyclin D1 and p27Kip1 expression." Journal of Biological Chemistry **283**(25): 17702-17711.

Orth, M., P. Metzger, S. Gerum, J. Mayerle, G. Schneider, C. Belka, M. Schnurr and K. Lauber (2019). "Pancreatic ductal adenocarcinoma: biological hallmarks, current status, and future perspectives of combined modality treatment approaches." Radiation Oncology **14**(1): 1-20.
Raimondi, C. and M. Falasca (2011). "Targeting PDK1 in Cancer." Current Medicinal Chemistry **18**(18): 2763-2769.

Rawla, P., T. Sunkara and V. Gaduputi (2019). "Epidemiology of Pancreatic Cancer: Global Trends, Etiology and Risk Factors." World Journal of Oncology **10**(1): 10-27.

Scheffzek K., M. R. A. and L. W. Kabsch W., * Alfred Lautwein,t Frank Schmitz, Alfred Wittinghofe (1997). "The Ras-RasGAP Complex: Structural Basis for GTPase Activation and Its Loss in Oncogenic Ras Mutants." Science **277**(5324): 333-338.

Schmidt, M., S. Fernandez de Mattos, A. van der Horst, R. Klompmaker, G. J. Kops, E. W. Lam, B. M. Burgering and R. H. Medema (2002). "Cell cycle inhibition by FoxO forkhead transcription factors involves downregulation of cyclin D." Molecular and Cellular Biology **22**(22): 7842-7852.

Schonhuber, N., B. Seidler, K. Schuck, C. Veltkamp, C. Schachtler, M. Zukowska, S. Eser, T. B. Feyerabend, M. C. Paul, P. Eser, S. Klein, A. M. Lowy, R. Banerjee, F. Yang, C. L. Lee, E. J. Moding, D. G. Kirsch, A. Scheideler, D. R. Alessi, I. Varela, A. Bradley, A. Kind, A. E. Schnieke, H. R. Rodewald, R. Rad, R. M. Schmid, G. Schneider and D. Saur (2014). "A next-generation dual-recombinase system for time- and host-specific targeting of pancreatic cancer." Nature Medicine **20**(11): 1340-1347.

Shen, W. H., A. S. Balajee, J. Wang, H. Wu, C. Eng, P. P. Pandolfi and Y. Yin (2007). "Essential role for nuclear PTEN in maintaining chromosomal integrity." Cell **128**(1): 157-170.

Shi, X., J. Wang, Y. Lei, C. Cong, D. Tan and X. Zhou (2019). "Research progress on the PI3K/AKT signaling pathway in gynecological cancer (Review)." Molecular Medicine Reports **19**(6): 4529-4535.

Stephens, L., K. Anderson and D. Stokoe (1998). "Protein Kinase B Kinases that Mediate PhosphatidylinositoI 3,4,5-TrisphosphateDependent Activation of Protein Kinase B." Science **Vol. 279**: 710-714.

Vermeulen, K. and R. Dirk (2003). "The cell cycle: a review of regulation, deregulation and therapeutic targets in cancer." Cell Proliferation **36**: 131–149.

Vigil, D., J. Cherfils, K. L. Rossman and C. J. Der (2010). "Ras superfamily GEFs and GAPs: validated and tractable targets for cancer therapy?" Nature Reviews Cancer **10**(12): 842-857.

Waddell, N., M. Pajic, A. M. Patch, D. K. Chang, K. S. Kassahn, P. Bailey, A. L. Johns, D. Miller, K. Nones, K. Quek, M. C. Quinn, A. J. Robertson, M. Z. Fadlullah, T. J. Bruxner, A. N. Christ, I. Harliwong, S. Idrisoglu, S. Manning, C. Nourse, E. Nourbakhsh, S. Wani, P. J. Wilson, E. Markham, N. Cloonan, M. J. Anderson, J. L. Fink, O. Holmes, S. H. Kazakoff, C. Leonard, F. Newell, B. Poudel, S. Song, D. Taylor, N. Waddell, S. Wood, Q. Xu, J. Wu, M. Pinese, M. J. Cowley, H. C. Lee, M. D. Jones, A. M. Nagrial, J. Humphris, L. A. Chantrill, V. Chin, A. M. Steinmann, A. Mawson, E. S. Humphrey, E. K. Colvin, A. Chou, C. J. Scarlett, A. V. Pinho, M. Giry-Laterriere, I. Rooman, J. S. Samra, J. G. Kench, J. A. Pettitt, N. D. Merrett, C. Toon, K. Epari, N. Q. Nguyen, A. Barbour, N. Zeps, N. B. Jamieson, J. S. Graham, S. P. Niclou, R. Bjerkvig, R. Grutzmann, D. Aust, R. H. Hruban, A. Maitra, C. A. Iacobuzio-Donahue, C. L. Wolfgang, R. A. Morgan, R. T. Lawlor, V. Corbo, C. Bassi, M. Falconi, G. Zamboni, G. Tortora, M. A. Tempero, I. Australian Pancreatic Cancer Genome, A. J. Gill, J. R. Eshleman, C. Pilarsky, A. Scarpa, E. A. Musgrove, J. V. Pearson, A. V. Biankin and S. M. Grimmond (2015). "Whole genomes redefine the mutational landscape of pancreatic cancer." Nature **518**(7540): 495-501.

Waters, A. M. and C. J. Der (2018). "KRAS: The Critical Driver and Therapeutic Target for Pancreatic Cancer." Cold Spring Harbor Perspectives in Medicine **8**(9): 1-17.

Wittenberg, A. D., S. Azar, A. Klochendler, M. Stolovich-Rain, S. Avraham, L. Birnbaum, A. Binder Gallimidi, M. Katz, Y. Dor and O. Meyuhas (2016). "Phosphorylated Ribosomal Protein S6 Is Required for Akt-Driven Hyperplasia and Malignant Transformation, but Not for Hypertrophy, Aneuploidy and Hyperfunction of Pancreatic beta-Cells." Plos One **11**(2): 1-25.

Ying, H., K. G. Elpek, A. Vinjamoori, S. M. Zimmerman, G. C. Chu, H. Yan, E. Fletcher-Sananikone, H. Zhang, Y. Liu, W. Wang, X. Ren, H. Zheng, A. C. Kimmelman, J. H. Paik, C. Lim, S. R. Perry, S. Jiang, B. Malinn, A. Protopopov, S. Colla, Y. Xiao, A. F. Hezel, N. Bardeesy, S. J. Turley, Y. A. Wang, L. Chin, S. P. Thayer and R. A. DePinho (2011). "PTEN is a major tumor suppressor in pancreatic ductal adenocarcinoma and regulates an NF-kappaB-cytokine network." Cancer Discovery **1**(2): 158-169.

Zhan, T., N. Rindtorff, J. Betge, M. P. Ebert and M. Boutros (2019). "CRISPR/Cas9 for cancer research and therapy." Seminars in Cancer Biology **55**: 106-119.

Zhang, F., Y. Wen and X. Guo (2014). "CRISPR/Cas9 for genome editing: progress, implications and challenges." Human Molecular Genetics **23**(R1): R40-46.

Zhao, X., S. Lu, J. Nie, X. Hu, W. Luo, X. Wu, H. Liu, Q. Feng, Z. Chang, Y. Liu, Y. Cao, H. Sun, X. Li, Y. Hu and Z. Yang (2014). "Phosphoinositide-dependent kinase 1 and mTORC2 synergistically maintain postnatal heart growth and heart function in mice." Molecular and Cellular Biology **34**(11): 1966-1975.